Partially pivoted ACA based acceleration of the energetic BEM for time-domain acoustic and elastic waves exterior problems

Partially pivoted ACA based acceleration of the Energetic BEM for time-domain acoustic and elastic waves exterior problems

A. Aimi[a], L. Desiderio[a,*], G. Di Credico[a]

[a] *Department of Mathematical, Physical and Computer Science, University of Parma, Parco Area delle Scienze, 53/A, Parma, Italy*

Abstract

We consider acoustic and elastic wave propagation problems in 2D unbounded domains, reformulated in terms of space-time Boundary Integral Equations (BIEs). For their numerical solution, we employ a weak formulation related to the energy of the system and we discretize the weak problems by a Galerkin-type Boundary Element Method (BEM): this approach, called Energetic BEM, has revealed accurate and stable even on large time intervals of analysis. In particular, it results that, when standard Lagrangian basis functions are considered, the BEM matrices have Toeplitz lower triangular block structure, where blocks for growing time become fully populated; hence the overall memory cost of the energetic BEM is $O(M^2N)$, M and N being the number of the space degrees of freedom and the total number of performed time steps, respectively. This drawback prevents the application of such method to large scale problems. As a possible remedy, we propose a fast technique based on the Adaptive Cross Approximation (ACA). The core of this procedure is the approximation of sufficiently large time blocks of the energetic BEM matrix through the partially pivoted ACA algorithm, which allows to compute only few of the original entries. This leads to reduced assembly time, which for the energetic BEM is generally relevant, coupled with reduced memory storage requirements. Additionally, the consequent acceleration of the matrix/vector multiplication together with a marching on time procedure, leads to remarkable reduction of the computational solution time. The effectiveness of the proposed method is theoretically proved and several numerical results are presented and discussed.

Keywords: Energetic Boundary Element Method, Adaptive Cross Approximation, Fast time-domain BEM, Wave Scattering Problems

1. Introduction

Numerical methods for solving acoustic and elastic wave propagation problems have widespread applications in industry, for instance in seismic exploration, target identification and geophysics. Computations in time-domain are of particular interest for problems beyond the reach of frequency-domain methods, such as the simulation of transient dynamics, moving sound sources or nonlinear and dynamical contact problems, since they allow to observe the phenomenon as it evolves. Even if different directions exist, the use of a Boundary Integral Equation (BIE) technique, whose discretization is known as the Boundary Element Method (BEM), is an appealing choice because it allows to handle problems defined on the exterior of bounded domains as easily as those defined in the interior, without the introduction of an artificial boundary to truncate the computational domain (see [21, 22]). Nevertheless, the applicability of Time-Domain BIE (TD-BIE) methods has been limited due to inefficiency and instability. Whereas the Galerkin discretization in space has been the de facto standard, no consensus has been reached yet on the numerical discretization in time, since only the weak formulation due to Bamberger and Ha Duong [11] furnishes genuine convergence results. Several other approaches have been proposed in literature, among which collocation [29], space-time Galerkin [1] and Convolution Quadrature (CQ) [26] are the most popular

*Corresponding author.

Email addresses: alessandra.aimi@unipr.it (A. Aimi), luca.desiderio@unipr.it (L. Desiderio), giulia.dicredico@unipr.it (G. Di Credico)

choices, although stability and convergence are assured under strong regularity assumptions on problem data.

Recently, a direct space-time Galerkin BEM for the discretization of TD-BIEs related to scalar and vector wave propagation problems has been introduced [2, 5] and compared with the classical space-time discretization approach due to Bamberger and Ha-Duong. The proposed technique is based on a natural energy identity satisfied by the solution of the corresponding differential problem, which leads to a space-time weak formulation of the BIEs with precise continuity and coerciveness properties [2]. Consequently, the integral problem can be discretized by unconditionally stable schemes with well-behaved stability constants even for large times. The algebraic reformulation of the energetic BEM leads to a linear system whose matrix has a Toeplitz lower-triangular block structure, where for growing time, blocks become fully populated, if standard Lagrangian basis functions are considered. Consequently, the overall memory cost of the energetic BEM is $O(M^2N)$, M and N being the number of the space degrees of freedom and the total number of time steps performed, respectively. This drawback prevents the application of such method to large scale problems.

Since the late 1980s, the development of fast numerical methods has improved the application of BEMs in the context of efficient and reliable simulations of wave propagation in unbounded exterior domains. Most early examples of such methods are the Fast Multiple Method (FMM) [23] and the Panel Clustering Method (PCM) [24]. Although these techniques are very effective and provide a valuable tool for the fast solution of BEM problems, their main disadvantage is that the knowledge of the kernel expansion is required in order to carry out the integration; all the terms of the series needed to reach a given accuracy must be computed in advance and then integrated, which can lead to a significant modification of the integration procedures in standard BEM codes. A complementary class of fast BEMs is based on hierarchical matrices ($\mathcal{H}$-matrices) [25] and approximation of their blocks through suitable algorithms, like interpolation and Adaptive Cross Approximation (ACA) [12]. These methods essentially are algebraic tools to approximate the BEM matrices, providing an alternative to tackle problems for which analytical expressions of the Green's functions are not available. Another possible approach is the wavelet based BEM [9], which produces sparse matrices based on orthogonal systems of wavelet like functions. All the above mentioned fast BEMs have been used to successfully simulate wave propagation phenomena in both frequency [6, 15, 17, 30] and time [14, 18, 20] domains.

In this paper, we consider 2D Dirichlet boundary value exterior problems defined by the acoustic and elastic wave equations, to which one can eventually reduce 3D problems invariant in one of the cartesian directions. For their solution, we propose a numerical scheme based on the energetic BEM, accelerated by the ACA technique. The core of this procedure is the approximation of sufficiently large time blocks of the energetic BEM matrix through the partially pivoted ACA algorithm, which allows to compute only few of the original entries. This leads to reduced assembly time, which for the energetic BEM is generally relevant, coupled with reduced memory storage requirements. Additionally, the consequent acceleration of the matrix/vector multiplication together with a marching on time procedure, leads to remarkable reduction of the computational solution time. The ACA algorithm was original developed for asymptotically smooth kernels, needing a suitable mesh elements clustering, and for this class of operators its convergence and performances were theoretically investigated and assessed [13]. Smooth kernels, like those involved in the energetic BEM after a double analytic integration in time variables and for sufficiently large times, do not formally fit into the definition of asymptotically smoothness. However, in this case the ACA algorithm can be interpreted as a rank-revealing decomposition applicable to kernels that admit degenerate approximations [12]. This enabled the successful application of ACA to energetic BEM, avoiding the construction of cluster trees.

The paper is organized as follows: in the next Section we present the model problems for the acoustic and elastic wave equations and their space-time boundary integral formulations. In Section 3 we describe the Energetic BEM discretization, focusing on its algebraic reformulation. Section 4 is devoted to the analysis of the time-integrated kernels generating matrix blocks entries and to briefly recall the ACA algorithm. Numerical results validating the proposed approach are illustrated and discussed in Section 5. Finally, some conclusions are drawn in the last Section.

2. Model problems and their boundary integral energetic formulation

In a fixed orthonormal Cartesian coordinates system $\mathbf{x} = (x_1, x_2)^\top$, we consider an open bounded domain $\Omega_0 \subset \mathbf{R}^2$ with a sufficiently smooth closed boundary $\Gamma := \partial\Omega_0$, and we denoted by $\Omega := \mathbf{R}^2 \setminus \Omega_0$ the exterior unbounded domain. We are interested in the numerical solution of the following time-domain wave propagation problem in Ω:

$$\begin{cases} \varrho\ddot{\mathbf{u}}(\mathbf{x};t) - \boldsymbol{\nabla}\cdot\boldsymbol{\sigma}[\mathbf{u}](\mathbf{x};t) = \mathbf{0} & (\mathbf{x};t) \in \Omega\times[0,T] \quad (2.1a)\\ \mathbf{u}(\mathbf{x};t) = \mathbf{g}(\mathbf{x};t) & (\mathbf{x};t) \in \Sigma_T := \Gamma\times[0,T] \quad (2.1b)\\ \mathbf{u}(\mathbf{x};0) = \mathbf{0} & \mathbf{x}\in\Omega \quad (2.1c)\\ \dot{\mathbf{u}}(\mathbf{x};0) = \mathbf{0} & \mathbf{x}\in\Omega, \quad (2.1d) \end{cases}$$

where $\mathbf{u} = (u_1, u_2)^\top$ denotes the unknown field of displacements, $\mathbf{g} = (g_1, g_2)^\top$ is the vector of the assigned boundary conditions of Dirichlet type and ϱ is the mass density. In problem (2.1), homogeneous initial conditions are assumed at the first time of interest $t = 0$. Furthermore, the superposed dot indicates time differentiation, while $\boldsymbol{\nabla}$ denotes the nabla operator.
The form of the Cauchy stress tensor $\boldsymbol{\sigma}[\mathbf{u}]$ determines the model and in this work we will consider both acoustic and elastic wave poropagation.

In order to approximate $\mathbf{u}$ through a BEM technique, we have to obtain a boundary integral reformulation of the problem (2.1). This can be done by using classical arguments and the knowledge of the fundamental solution of the two-dimensional differential operator at hand. In the case of wave propagation in a homogenous unbounded domain, the full-space fundamental solution $\mathbf{G}(\mathbf{x},\mathbf{y};t,\tau)$ for the displacement in time-domain is found as the solution of the equation

$$\varrho\ddot{\mathbf{G}}(\mathbf{x},\mathbf{y};t,\tau) - \boldsymbol{\nabla}\cdot\boldsymbol{\sigma}[\mathbf{G}](\mathbf{x},\mathbf{y};t,\tau) = \mathbf{I}\delta(\mathbf{x}-\mathbf{y})\delta(t-\tau), \tag{2.2}$$

$\mathbf{I}$ being the 2-by-2 identity tensor and $\delta(\cdot)$ the Dirac distribution. We remark that $\mathbf{G}(\mathbf{x},\mathbf{y};t,\tau)$ is a tensor field with the doubly indexed components $G_{ij}(\mathbf{x},\mathbf{y};t,\tau)$, for $i,j = 1,2$.

The knowledge of the fundamental solution allows us to consider the following single layer potential representation of the solution of problem (2.1), written by components as:

$$u_i(\mathbf{x},t) = \sum_{j=1}^{2}\int_0^t\int_\Gamma G_{ij}(\mathbf{x},\mathbf{y};t,\tau)\varphi_j(\mathbf{y},\tau)d\Gamma_{\mathbf{y}}d\tau, \quad \mathbf{x}\in\Omega\setminus\Gamma,\ t\in[0,T], \quad i=1,2. \tag{2.3}$$

where $\boldsymbol{\varphi} = (\varphi_1,\varphi_2)^\top$ is a suitable density field to be determined. From the above formula, with a limiting process that makes a point $\mathbf{x}\in\Omega$ tending to a point $\mathbf{x}\in\Gamma$ and exploiting the Dirichlet boundary condition, we can obtain a system of two TD-BIEs:

$$g_i(\mathbf{x},t) = \sum_{j=1}^{2}\int_0^t\int_\Gamma G_{ij}(\mathbf{x},\mathbf{y};t,\tau)\varphi_j(\mathbf{y},\tau)d\Gamma_{\mathbf{y}}d\tau =: \sum_{j=1}^{2}\left(V_{ij}\varphi_j\right)(\mathbf{x},t), \quad (\mathbf{x},t)\in\Sigma_T,\ i=1,2. \tag{2.4}$$

The space-time integral operators $V_{ij} : L^2((0,T];H^{-1/2}(\Gamma)) \longrightarrow H^1((0,T];H^{1/2}(\Gamma))$, depending on the components of the fundamental solution, allow us to rewrite the boundary equations system in a vectorial form:

$$\left(\begin{bmatrix} V_{11} & V_{12}\\ V_{21} & V_{22}\end{bmatrix}\begin{bmatrix}\varphi_1\\ \varphi_2\end{bmatrix}\right)(\mathbf{x},t) = \begin{bmatrix} g_1\\ g_2\end{bmatrix}(\mathbf{x},t). \tag{2.5}$$

This BIEs system is the core of the entire method: its numerical resolution generates an approximation of vector $\boldsymbol{\varphi}$ that can be used in the representation formula (2.3), recovering in a post-processing phase the behaviour of the displacement $\mathbf{u}$ at each point of the diffusion domain and at each time instant.

Now we write the energetic weak formulation of the BIEs (2.5) (see [2] and [5] for further details):

find $\varphi_i \in L^2([0,T]; H^{-1/2}(\Gamma)), i = 1,2$ *such that*

$$\sum_{j=1}^{2} < (\dot{V_{ij}}\varphi_j), \psi_i >_{L^2(\Sigma_T)} = < \dot{g}_i, \psi_i >_{L^2(\Sigma_T)} \quad \forall \psi_i \in L^2([0,T]; H^{-1/2}(\Gamma)), \quad i = 1,2. \tag{2.6}$$

2.1. Acoustics

At first we are interested in the numerical solution of an acoustic wave propagation problem, i.e. we consider

$$\boldsymbol{\sigma}(\mathbf{x};t) := \varrho c^2 \boldsymbol{\nabla}\mathbf{u}(\mathbf{x};t), \tag{2.7}$$

where $c > 0$ is the speed of the wave propagation. In this case equation (2.1a) can be written as the vector acoustic wave equation:

$$\ddot{\mathbf{u}}(\mathbf{x};t) - c^2 \boldsymbol{\Delta}\mathbf{u}(\mathbf{x};t) = \mathbf{0} \qquad (\mathbf{x};t) \in \Omega \times [0,T], \tag{2.8}$$

$\boldsymbol{\Delta}$ being the vector Laplace operator, and the component of the tensor $\mathbf{G}(\mathbf{x},\mathbf{y};t,\tau)$ are given by:

$$G_{ij}(\mathbf{x},\mathbf{y};t,\tau) := \frac{c}{2\pi} \frac{H(c(t-\tau)-r)}{\sqrt{c^2(t-\tau)^2 - r^2}} \delta_{ij} \qquad \text{with } r := \|\mathbf{r}\|_2 := \|\mathbf{x}-\mathbf{y}\|_2, \qquad i,j = 1,2, \tag{2.9}$$

where $H(\cdot)$ denotes the Heaviside step function while δ_{ij} indicates the Kronecker symbol. Consequently, the components of the unknown density $\boldsymbol{\varphi}$ decouple, since equation (2.5) is recast in the following form:

$$\left(\begin{bmatrix} V & 0 \\ 0 & V \end{bmatrix} \begin{bmatrix} \varphi_1 \\ \varphi_2 \end{bmatrix} \right)(\mathbf{x},t) = \begin{bmatrix} g_1 \\ g_2 \end{bmatrix}(\mathbf{x},t) \qquad \text{with} \qquad V := V_{11} = V_{22}. \tag{2.10}$$

Thus, we can retrieve the vector field $\boldsymbol{\varphi}$ by solving one scalar BIE with two different right hand sides.

Having introduced the energy of the wave equation (2.8) as follows (see [2])

$$\mathcal{E}(\mathbf{u};t) := \frac{1}{2} \sum_{i=1}^{2} \left(\int_\Omega \dot{u_i}^2(\mathbf{x};t) \mathrm{d}\mathbf{x} + c^2 \sum_{j=1}^{2} \int_\Omega \left| \frac{\partial u_i}{\partial x_j}(\mathbf{x};t) \right|^2 \mathrm{d}\mathbf{x} \right), \tag{2.11}$$

it turns out that the quadratic form related to the left-hand side of the energetic weak problem (2.6) satisfies

$$\mathcal{E}(\mathbf{u};T) = \sum_{i=1}^{2} \int_\Gamma \int_0^T (\dot{V_{ii}}\varphi_i)(\mathbf{x},t)\varphi_i(\mathbf{x},t) dt d\Gamma_{\mathbf{x}}, \qquad i = 1,2. \tag{2.12}$$

2.2. Elastodynamics

As second model we consider an elastic wave propagation problem, corresponding to

$$\boldsymbol{\sigma}[\mathbf{u}](\mathbf{x};t) := \lambda \left[\boldsymbol{\nabla} \cdot \mathbf{u}(\mathbf{x};t)\right] \mathbf{I} + \mu \left[\boldsymbol{\nabla}\mathbf{u}(\mathbf{x};t) + \boldsymbol{\nabla}\mathbf{u}^\top(\mathbf{x};t)\right], \tag{2.13}$$

where μ is the shear modulus and λ is the Lamé parameter. These last two quantities are related to the Poisson ratio ν by $\lambda := 2\mu\nu(1-2\nu)^{-1}$. Thus, equation (2.1a) takes the following form

$$\ddot{\mathbf{u}}(\mathbf{x};t) - c_{\mathrm{S}}^2 \boldsymbol{\Delta}\mathbf{u}(\mathbf{x};t) - (c_{\mathrm{P}}^2 - c_{\mathrm{S}}^2)\boldsymbol{\nabla}(\boldsymbol{\nabla} \cdot \mathbf{u}(\mathbf{x};t)) = \mathbf{0} \qquad (\mathbf{x};t) \in \Omega \times [0,T]. \tag{2.14}$$

For this model there are two wave speeds, $c_{\mathrm{P}}^2 := (\lambda + 2\mu)\varrho^{-1}$ and $c_{\mathrm{S}}^2 := \mu\varrho^{-1}$, which are associated with the pressure wave and the shear wave. Since for any real materials, the shear modulus and the Lamé parameter are both real positive quantities, it holds $c_{\mathrm{P}} > c_{\mathrm{S}}$, i.e. the pressure waves

travel faster than the shear ones. Consequently, the former is called Primary wave (P-wave in short), while the latter is called Secondary wave (S-wave in short). Additionally, when Poisson's relation is satisfied, i.e. $\lambda = \mu$, we have $c_{\mathrm{P}} = \sqrt{3}c_{\mathrm{S}}$.

As in the previous scalar acoustic case, the second order tensor fundamental solution associated to the differential operator in (2.14) is known in closed form (see [10]) and its components are given by:

$$\begin{aligned} G_{ij}(\mathbf{x},\mathbf{y};t,\tau) :=& \frac{H[c_{\mathrm{P}}(t-\tau)-r]}{2\pi\rho c_{\mathrm{P}}} \left\{ \frac{r_i r_j}{r^4} \frac{2c_{\mathrm{P}}^2(t-\tau)^2 - r^2}{\sqrt{c_{\mathrm{P}}^2(t-\tau)^2 - r^2}} - \frac{\delta_{ij}}{r^2}\sqrt{c_{\mathrm{P}}^2(t-\tau)^2 - r^2} \right\} \\ & - \frac{H[c_{\mathrm{S}}(t-\tau)-r]}{2\pi\rho c_{\mathrm{S}}} \left\{ \frac{r_i r_j}{r^4} \frac{2c_{\mathrm{S}}^2(t-\tau)^2 - r^2}{\sqrt{c_{\mathrm{S}}^2(t-\tau)^2 - r^2}} - \frac{\delta_{ij}}{r^2} \frac{c_{\mathrm{S}}^2(t-\tau)^2}{\sqrt{c_{\mathrm{S}}^2(t-\tau)^2 - r^2}} \right\}, \quad i,j = 1,2, \end{aligned} \tag{2.15}$$

where the Heaviside function models the primary and the secondary wave fronts propagation. In this case, the components of the unknown density $\boldsymbol{\varphi}$ do not decouple and equation (2.5) still represents a system of two BIEs.

It can be proved also for the elastic model that, having defined the energy of the system as (see [5])

$$\mathcal{E}(\mathbf{u};t) := \frac{1}{2}\sum_{i=1}^{2}\left(\int_{\Omega} \dot{u}_i^2(\mathbf{x};t)d\mathbf{x} + c_{\mathrm{S}}^2 \sum_{j=1}^{2} \int_{\Omega} \left| \frac{\partial u_i}{\partial x_j}(\mathbf{x};t) \right|^2 + (c_{\mathrm{P}}^2 - c_{\mathrm{S}}^2) \sum_{j=1}^{2} \int_{\Omega} \frac{\partial u_i}{\partial x_i}(\mathbf{x};t) \frac{\partial u_j}{\partial x_j}(\mathbf{x};t) d\mathbf{x} \right), \tag{2.16}$$

it holds

$$\mathcal{E}(\mathbf{u};T) = \sum_{i,j=1}^{2} \int_0^T \int_{\Gamma} (\dot{V_{ij}\varphi_j})(\mathbf{x};t)\varphi_i(\mathbf{x};t) d\Gamma_{\mathbf{x}} dt. \tag{2.17}$$

3. Energetic BEM discretization

For the discretization phase, we consider an uniform decomposition of the time interval $[0,T]$ with time step $\Delta t := T/N$, N being a positive integer, generated by $N+1$ instants:

$$t_n := n\Delta t, \qquad n = 0,\ldots,N \tag{3.1}$$

and we choose temporally piecewise constant shape functions, although higher degree shape functions can be used. Note that, for this particular choice, the shape functions, denoted by $\widehat{w}_n(t)$, are defined as:

$$\widehat{w}_n(t) := H(t-t_n) - H(t-t_{n+1}), \qquad n = 0,\ldots,N-1. \tag{3.2}$$

For the space discretization, we consider a boundary mesh $\mathcal{T}_{\Delta x}(\Gamma) := \{e_1,\ldots,e_M\}$ constituted by M flat segments such that $\mathrm{length}(e_i) \leq \Delta x$, $e_i \cap e_j = \varnothing$ if $i \neq j$ and $\cup_{i=1}^{M} e_i$ coincides with $\overline{\Gamma}$ if the boundary is polygonal, or it is a suitable approximation of $\overline{\Gamma}$, otherwise.
The functional background compels one to choose spatially shape functions belonging to $L^2(\Gamma)$. Hence, we consider piecewise constant basis functions $w_m(\mathbf{x})$, $m = 1,\ldots,M$ related to $\mathcal{T}_{\Delta x}(\Gamma)$.

Thus, the unknown approximate solution of problem (2.6) is expressed as:

$$\varphi_i(\mathbf{x};t) \simeq \sum_{n=0}^{N-1} \widehat{w}_n(t) \sum_{m=1}^{M} \alpha_{i,m}^{(n)} w_m(\mathbf{x}) \qquad i = 1,2, \tag{3.3}$$

and the test function are replaced by $\psi_i(\mathbf{x};t) = w_{\widetilde{m}}(\mathbf{x})\widehat{w}_{\widetilde{n}}(t)$. Consequently, the energetic BEM

discretization produces the linear system

$$\mathbb{E}\boldsymbol{\alpha} = \boldsymbol{\beta}, \tag{3.4}$$

where the matrix $\mathbb{E}$ has a block lower triangular Toeplitz structure, since its elements depend on the difference $\Delta_{\tilde{n},n} := t_{\tilde{n}} - t_n$ and in particular they vanish if $t_{\tilde{n}} < t_n$. Hence, if we set $n = 0$ so that we denote by $\mathbb{E}^{(\ell)}$ the block obtained when $t_\ell := \Delta_{\tilde{n},n} = t_{\tilde{n}}$, with $\ell = \tilde{n} = 0, \dots, N-1$, the linear system (3.4) can be written as

$$\begin{pmatrix} \mathbb{E}^{(0)} & 0 & 0 & \dots & 0 \\ \mathbb{E}^{(1)} & \mathbb{E}^{(0)} & 0 & \dots & 0 \\ \mathbb{E}^{(2)} & \mathbb{E}^{(1)} & \mathbb{E}^{(0)} & \dots & 0 \\ \vdots & \vdots & \vdots & \ddots & \vdots \\ \mathbb{E}^{(N-1)} & \mathbb{E}^{(N-2)} & \mathbb{E}^{(N-3)} & \dots & \mathbb{E}^{(0)} \end{pmatrix} \begin{pmatrix} \boldsymbol{\alpha}^{(0)} \\ \boldsymbol{\alpha}^{(1)} \\ \boldsymbol{\alpha}^{(2)} \\ \vdots \\ \boldsymbol{\alpha}^{(N-1)} \end{pmatrix} = \begin{pmatrix} \boldsymbol{\beta}^{(0)} \\ \boldsymbol{\beta}^{(1)} \\ \boldsymbol{\beta}^{(2)} \\ \vdots \\ \boldsymbol{\beta}^{(N-1)} \end{pmatrix} \tag{3.5}$$

where the unknowns and right hand side entries are organized as follows

$$\begin{aligned} \boldsymbol{\alpha}^{(\ell)} &= \left(\alpha^{(\ell)}_{1,1}, \alpha^{(\ell)}_{1,2}, \dots, \alpha^{(\ell)}_{1,M}, \alpha^{(\ell)}_{2,1}, \alpha^{(\ell)}_{2,2}, \dots, \alpha^{(\ell)}_{2,M}\right)^\top \\ \boldsymbol{\beta}^{(\ell)} &= \left(\beta^{(\ell)}_{1,1}, \beta^{(\ell)}_{1,2}, \dots, \beta^{(\ell)}_{1,M}, \beta^{(\ell)}_{2,1}, \beta^{(\ell)}_{2,2}, \dots, \beta^{(\ell)}_{2,M}\right)^\top, \end{aligned} \tag{3.6}$$

while the $2M$-by-$2M$ block $\mathbb{E}^{(\ell)}$ has the following structure

$$\mathbb{E}^{(\ell)} = \begin{pmatrix} \mathbb{E}^{(\ell)}_{11} & \mathbb{E}^{(\ell)}_{12} \\ \mathbb{E}^{(\ell)}_{21} & \mathbb{E}^{(\ell)}_{22} \end{pmatrix} \qquad \text{with} \quad \mathbb{E}^{(\ell)}_{12} = \mathbb{E}^{(\ell)}_{21}. \tag{3.7}$$

The solution of (3.5) is obtained by a block forward substitution, i.e. at every time instant t_ℓ with $\ell = 0, \dots, N-1$, one computes

$$\mathbf{z}^{(\ell)} = \boldsymbol{\beta}^{(\ell)} - \sum_{j=1}^{\ell} \mathbb{E}^{(j)} \boldsymbol{\alpha}^{(\ell-j)} \tag{3.8}$$

and then solves the reduced linear system

$$\mathbb{E}^{(0)} \boldsymbol{\alpha}^{(\ell)} = \mathbf{z}^{(\ell)}. \tag{3.9}$$

Procedure (3.8)-(3.9) is a time-marching technique, where the only matrix to be inverted is the non-singular block $\mathbb{E}^{(0)}$; therefore the LU factorization needs to be performed only once and stored. All the other blocks $\mathbb{E}^{(\ell)}$ are used to update at every time step the right-hand side. Of course, due to the whole matrix $\mathbb{E}$ structure, one can construct and store only blocks $\mathbb{E}^{(0)}, \dots, \mathbb{E}^{(N-1)}$ with a preliminary reduction in the computational cost and the memory requirement.
Finally, we stress that the crucial point for the success of the energetic BEM is the careful numerical evaluation of the entries of the block $\mathbb{E}^{(0)}$ that must take place under the assumption that all the involved integrals are computed with a sufficiently high accuracy.

3.1. Acoustics

For what concerns the discretization of the energetic weak problem related to the acoustic model, we remark that the block $\mathbb{E}^{(\ell)}$ inherits the structure of the space-time integral operator $\mathbf{V}$ so that, due to (2.10), we have:

$$\mathbb{E}^{(\ell)} = \begin{pmatrix} \mathbb{E}^{(\ell)} & 0 \\ 0 & \mathbb{E}^{(\ell)} \end{pmatrix} \qquad \text{with} \quad \mathbb{E}^{(\ell)} := \mathbb{E}^{(\ell)}_{11} = \mathbb{E}^{(\ell)}_{22}. \tag{3.10}$$

After a double analytic integration in the time variables, the entries of the M-by-M matrix $\mathbb{E}^{(\ell)}$

are of the form:

$$\mathbb{E}^{(\ell)}_{\tilde{m},m} = -\frac{1}{2\pi}\sum_{\tilde{\eta},\eta=0}^{1}(-1)^{\tilde{\eta}+\eta}\int_{\Gamma} w_{\tilde{m}}(\mathbf{x})\int_{\Gamma} w_m(\mathbf{y})\mathcal{V}(\mathbf{x},\mathbf{y};\Delta_{\tilde{n}+\tilde{\eta},\eta})\mathrm{d}\Gamma_{\mathbf{y}}\mathrm{d}\Gamma_{\mathbf{x}}, \tag{3.11}$$

where

$$\mathcal{V}(\mathbf{x},\mathbf{y};t) = H(ct-r)\zeta(\mathbf{x},\mathbf{y};t;c) \tag{3.12}$$

with peculiar kernel function

$$\zeta(\mathbf{x},\mathbf{y};t;c) := \left[\log\left(ct+\sqrt{c^2t^2-r^2}\right)-\log(r)\right] \tag{3.13}$$

In (3.12), the Heaviside function represents the wave front propagation and its contribution is 0 or 1. Moreover, in (3.13) we observe a space singularity of type $\mathcal{O}(\log(r))$ as $r\to 0$, which is typical of the weakly singular kernels related to 2D elliptic problems.

3.2. Elastodynamics

When we deal with elastic problems, all the four M-by-M sub-blocks $\mathbb{E}^{(\ell)}_{ij}$, with $i,j=1,2$, in (3.7) are non-zero and, after a double analytical integration in time variables, their generic entry for $i,j=1,2$ has the form

$$\left(\mathbb{E}^{(\ell)}_{ij}\right)_{\tilde{m},m} = -\frac{1}{2\pi\varrho}\sum_{\tilde{\eta},\eta=0}^{1}(-1)^{\tilde{\eta}+\eta}\int_{\Gamma} w_{\tilde{m}}(\mathbf{x})\int_{\Gamma} w_m(\mathbf{y})\mathcal{V}_{ij}(\mathbf{x},\mathbf{y};\Delta_{\tilde{n}+\tilde{\eta},\eta})d\Gamma_{\mathbf{x}}d\Gamma_{\mathbf{y}}, \tag{3.14}$$

where

$$\begin{aligned}\mathcal{V}_{ij}(\mathbf{x},\mathbf{y};t) := &\left(\frac{r_ir_j}{r^4}-\frac{\delta_{ij}}{2r^2}\right)\left[\frac{H(c_{\mathrm{P}}t-r)}{c_{\mathrm{P}}^2}\xi(\mathbf{x},\mathbf{y};t;c_{\mathrm{P}})-\frac{H(c_{\mathrm{S}}t-r)}{c_{\mathrm{S}}^2}\xi(\mathbf{x},\mathbf{y};t;c_{\mathrm{S}})\right]\\ &+\frac{\delta_{ij}}{2}\left[\frac{H(c_{\mathrm{P}}t-r)}{c_{\mathrm{P}}^2}\zeta(\mathbf{x},\mathbf{y};t;c_{\mathrm{P}})+\frac{H(c_{\mathrm{S}}t-r)}{c_{\mathrm{S}}^2}\zeta(\mathbf{x},\mathbf{y};t;c_{\mathrm{S}})\right]\end{aligned} \tag{3.15}$$

having introduced, besides (3.13), another peculiar kernel function

$$\xi(\mathbf{x},\mathbf{y};t;c) := ct\sqrt{c^2t^2-r^2}. \tag{3.16}$$

If $0\le r\le c_{\mathrm{S}}t<c_{\mathrm{P}}t$ the kernel $\mathcal{V}_{ij}$ has a reduced form:

$$\mathcal{V}_{ij}(\mathbf{x},\mathbf{y};t) = \left(\frac{r_ir_j}{r^2}-\frac{\delta_{ij}}{2}\right)\frac{(c_{\mathrm{P}}^2-c_{\mathrm{S}}^2)t^2}{c_{\mathrm{P}}c_{\mathrm{S}}\left[\xi(\mathbf{x},\mathbf{y};t;c_{\mathrm{S}})+\xi(\mathbf{x},\mathbf{y};t;c_{\mathrm{P}})\right]}+\frac{\delta_{ij}}{2}\left[\frac{\zeta(\mathbf{x},\mathbf{y};t;c_{\mathrm{P}})}{c_{\mathrm{P}}^2}+\frac{\zeta(\mathbf{x},\mathbf{y};t;c_{\mathrm{S}})}{c_{\mathrm{S}}^2}\right], \tag{3.17}$$

with a space weak singularity of type $\mathcal{O}(\log(r))$ for $r\longrightarrow 0$, as highlighted for acoustic problems. Instead, if $c_{\mathrm{S}}t<r\le c_{\mathrm{P}}t$, the reduced form of the kernel $\mathcal{V}_{ij}$ is

$$\mathcal{V}_{ij}(\mathbf{x},\mathbf{y};t) = \left(\frac{r_ir_j}{r^4}-\frac{\delta_{ij}}{2r^2}\right)\frac{\xi(\mathbf{x},\mathbf{y};t;c_{\mathrm{P}})}{c_{\mathrm{P}}^2}+\frac{\delta_{ij}}{2}\frac{\zeta(\mathbf{x},\mathbf{y};t;c_{\mathrm{P}})}{c_{\mathrm{P}}^2}, \tag{3.18}$$

with no space singularity, due to the fact that r is neither null nor negligible in this interval.

Quadrature schemes for the efficient evaluation of all the above integrals can be found in [2, 8].

Remark. The proposed energetic weak formulation, after time integration, can be regarded as a Newmark scheme with parameters $\zeta = 1/2$ and $\theta = 1$ in the notation of [28], as proved for scalar problems in [3, 4] in the more general framework of Energetic BEM-FEM coupling. This particular Newmark scheme is implicit, unconditionally stable and first-order accurate in Δt. Furthermore, the theoretical analysis about convergence and space-time accuracy in the context of elastodynamic problems has been performed in [7]. The theoretical results will be mantained

also after the coupling with the ACA based compession technique, introduced in the following, as shown by the intensive numerical tests presented in Section 5.

4. Partially pivoted ACA based fast blocks generation

Depending on the value of wave propagation speed, the wavefront can quickly recover the obstacle or not. In the first case, blocks $\mathbb{E}^{(\ell)}$ in (3.5) becomes immediately full matrices, while in the latter case first time blocks are highly sparse, but, due to the Heaviside function in the kernels, modeling wavefront propagation, for growing index ℓ, i.e. as time goes on, they become more and more populated until they assume a full structure, too. These two scenarios are shown in Figure 1 for the acoustic model, where blocks structure is compared at the same time instants for two different speeds. Consequently, the whole memory storage requirement for the matrix $\mathbb{E}$ in (3.4) has to be considered as $\mathcal{O}(M^2N)$. The above drawback reduces the efficiency of the energetic BEM. In this regard, we propose a procedure to reduce the computational time and cost for the generation of the full blocks $\mathbb{E}^{(\ell)}$, based on a subtler analysis of their entries, while sparse blocks do not need to be compressed. For sake of simplicity, we focus our attention on the acoustic problem but the analysis we are going to explain can be extended to the elastic case, as we will show at the end of this section.

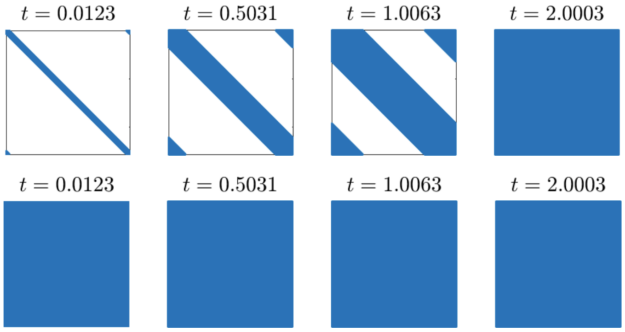

Figure 1: Structure of the block $\mathbb{E}^{(\ell)}$ at different time instants. Here, we consider a circumference Γ with unitary radius, approximated by $M = 512$ segments with length $\Delta x = \pi/256$, so that $\mathbb{E}^{(\ell)}$ is a 512-by-512 matrix. The problems evolves in the time interval $[0, 8\pi]$, decomposed uniformly with $N = 2048$ instants and characterized by the velocities $c = 1$ (top plot) and $c = 343$ (bottom plot).

4.1. Acoustics

When, for growing times, it becomes $c\,t_{\ell-1} > r$, then (3.11) reduces to

$$\mathbb{E}^{(\ell)}_{\tilde{m},m} = -\frac{1}{2\pi}\int_{\Gamma} w_{\tilde{m}}(\mathbf{x}) \int_{\Gamma} w_m(\mathbf{y})\widetilde{\mathcal{V}}(\mathbf{x},\mathbf{y};t_\ell)\mathrm{d}\Gamma_{\mathbf{y}}\mathrm{d}\Gamma_{\mathbf{x}} \tag{4.1}$$

where

$$\widetilde{\mathcal{V}}(\mathbf{x},\mathbf{y};t) = \log\left(\frac{\left(ct+\sqrt{c^2t^2-r^2}\right)^2}{\left(c(t-\Delta t)+\sqrt{c^2(t-\Delta t)^2-r^2}\right)\left(c(t+\Delta t)+\sqrt{c^2(t+\Delta t)^2-r^2}\right)}\right) \tag{4.2}$$

Thus, when $ct_{\ell-1} > diam(\Gamma)$, we do not observe any space singularity, since the kernel function $\widetilde{\mathcal{V}}(\mathbf{x},\mathbf{y};t_\ell)$ is smooth for $r \to 0$; further we note that it is symmetric in space variables and in the limit for $t \to \infty$ it tends to become identically zero.

The reduction of the memory storage for the fully populated blocks $\mathbb{E}^{(\ell)}$, generated by the energetic BEM, rests on the possibility that the kernel $\widetilde{\mathcal{V}}(\mathbf{x},\mathbf{y};t)$ admits a low-rank or degenerate expansion, i.e. it can be decomposed as follows:

$$\widetilde{\mathcal{V}}(\mathbf{x},\mathbf{y};t) = \sum_{k=0}^{k^*_\ell} \chi_k(\mathbf{x};t)\omega_k(\mathbf{y};t) + R_{k^*_\ell}(\mathbf{x},\mathbf{y};t) := S_{k^*_\ell}(\mathbf{x},\mathbf{y};t) + R_{k^*_\ell}(\mathbf{x},\mathbf{y};t), \tag{4.3}$$

where $R_{k_\ell^*}(\mathbf{x},\mathbf{y};t)$ is the residuum that tends to zero for $k_\ell^* \to \infty$, k_ℓ^* being the rank of the representation. Going back to the definition (4.2) and to the properties of smoothness and symmetry of $\widetilde{\mathcal{V}}(\mathbf{x},\mathbf{y};t)$, for a fixed t and Δt, it is well known (see [31]) that such kind of kernels can be represented by a bilinear expansion in terms of eigenvalues and eigenfunctions in space variables. Anyway, it is better to work in the r variable to have an idea of the value of the rank k_ℓ^* in the degenerate decomposition (4.3). Here, we stress that the following theoretical study is not necessary for the implementation of the method, since we will employ a rank revealing algorithm for the computation of the low-rank approximation of the matrices $\mathbb{E}^{(\ell)}$.

Taking into account the definition of the reduced integral kernel (4.2) and the fact that the shape functions in (4.1) are piecewise constant, a generic matrix element can be approximated as follows:

$$\mathbb{E}^{(\ell)}_{\tilde{m},m} \simeq -\frac{\Delta x^2}{2\pi}\widetilde{\mathcal{V}}(r;t_\ell) \tag{4.4}$$

since the function $\widetilde{\mathcal{V}}(\mathbf{x},\mathbf{y};t_\ell)$ is almost flat in r for a large time instant t_ℓ. We proceed then in the estimate by applying to this smooth kernel a Taylor expansion in the r variable, centred in $r=0$:

$$\mathbb{E}^{(\ell)}_{\tilde{m},m} \simeq \sum_{k=0}^{+\infty} C_k(t_\ell) r^{2k} = \left(S_{k_\ell^*}(r;t_\ell) + R_{k_\ell^*}(r;t_\ell)\right), \tag{4.5}$$

where $S_{k_\ell^*}(r;t_\ell)$ and $R_{k_\ell^*}(r;t_\ell)$ represent the summation over the first k_ℓ^*+1 terms of the series and the related reminder, respectively. In particular, the coefficients $C_k(t)$ can be approximated, up to negligible terms for large t, as follows:

$$C_k(t) \simeq \widetilde{C}_k(t) := -\frac{(c\Delta x\,\Delta t)^2}{2\pi}\frac{(2k+1)!}{(k!)^2 4^k}\frac{1}{(ct)^{2k+2}}. \tag{4.6}$$

Now, if we introduce the function

$$\widetilde{S}_{k_\ell^*}(r;t) := \sum_{k=0}^{k_\ell^*} \widetilde{C}_k(t) r^{2k} \tag{4.7}$$

and we observe that, since for each $k \geq 0$ it holds

$$\frac{(2k+1)(2k+1)}{2k+1}\frac{r^{2k}}{(ct)^{2k+2}} = -\frac{1}{c(2k+1)}\frac{\partial^2}{\partial t \partial r}\left(\frac{r^{2k+1}}{(ct)^{2k+1}}\right),$$

we have:

$$\begin{aligned}\widetilde{S}_{k_\ell^*}(r;t) &= \frac{c(\Delta x\,\Delta t)^2}{2\pi}\sum_{k=0}^{k_\ell^*}\frac{(2k)!}{(2k+1)(k!)^2 4^k}\frac{\partial^2}{\partial t\partial r}\left(\frac{r^{2k+1}}{(ct)^{2k+1}}\right)\\ &= \frac{c(\Delta x\,\Delta t)^2}{2\pi}\frac{\partial^2}{\partial t\partial r}\left[\sum_{k=0}^{k_\ell^*}\frac{(2k)!}{(2k+1)(k!)^2 4^k}\left(\frac{r}{ct}\right)^{2k+1}\right].\end{aligned} \tag{4.8}$$

The argument of the double derivative in formula (4.8) is the general term, calculated in $x = r/(ct)$, of the expansion centred in $x=0$ of the function $\arcsin(x)$. Therefore, we approximate the generic block element in (4.5) with a series of terms (4.8), having as limit for $k_\ell^* \to +\infty$ the following function:

$$\widetilde{S}_\infty(r;t) = \frac{c(\Delta x\,\Delta t)^2}{2\pi}\left[\frac{\partial^2}{\partial t\partial r}\arcsin\left(\frac{r}{ct}\right)\right] = -\frac{c(\Delta x\,\Delta t)^2}{2\pi}\left(\frac{1}{t\sqrt{c^2t^2-r^2}} + \frac{r^2}{t\sqrt{(c^2t^2-r^2)^3}}\right). \tag{4.9}$$

Consequently, we can estimate the reminder $R_{k_\ell^*}(r;t)$ at a fixed k_ℓ^* with the difference

$$R_{k_\ell^*}(r;t) \simeq \widetilde{S}_\infty(r;t) - \widetilde{S}_{k_\ell^*}(r;t). \tag{4.10}$$

Thus, we can conclude that it is possible to obtain a low-rank approximation of the matrix $\mathbb{E}^{(\ell)}$ and k_ℓ^* is the rank required to achieve a given relative accuracy $\varepsilon > 0$ if

$$\left|R_{k_\ell^*}(r;t_\ell)\right| \simeq \left|\widetilde{S}_\infty(r;t_\ell) - \widetilde{S}_{k_\ell^*}(r;t_\ell)\right| \leq \varepsilon \left|\widetilde{S}_\infty(r;t_\ell)\right|. \tag{4.11}$$

At the discrete level, the decomposition (4.5) can be written as

$$\mathbb{E}^{(\ell)} = \mathbb{S}_{k_\ell^*} + \mathbb{R}_{k_\ell^*} \qquad \text{with} \quad \mathbb{S}_{k_\ell^*} := \mathbb{Q} \cdot \mathbb{W}^\top, \tag{4.12}$$

where $\mathbb{Q}$ and $\mathbb{W}$ are both M-by-k_ℓ^* matrices and the residuum $\mathbb{R}_{k_\ell^*}$ is such that

$$\left\|\mathbb{R}_{k_\ell^*}\right\|_{\mathrm{F}} = \left\|\mathbb{E}^{(\ell)} - \mathbb{S}_{k_\ell^*}\right\|_{\mathrm{F}} = \left\|\mathbb{E}^{(\ell)} - \mathbb{Q} \cdot \mathbb{W}^\top\right\|_{\mathrm{F}} \leq \varepsilon \left\|\mathbb{E}^{(\ell)}\right\|_{\mathrm{F}},$$

where $\|\cdot\|_{\mathrm{F}}$ denotes the Frobenius norm of a real matrix and $\varepsilon > 0$ is a parameter representing the accuracy required to the approximation.

It is worth noting that such low-rank approximation can be computed by different algorithms. In general, the best low-rank representation up to a given accuracy can be found through the Singular Value Decomposition (SVD) but this technique is unattractive for large-scale computations since, due to the computational complexity, it can not lead to fast procedures. On the other hand, a purely algebraic algorithm as the partially pivoted Adaptive Cross Approximation (ACA) (see [12, 13]) appears to be very efficient for the application to the energetic BEM matrices, because it allows to attain the low-rank representation of the blocks $\mathbb{E}^{(\ell)}$ by computing adaptively some of the rows and the columns of the original matrix, until a stopping criterion related to the set accuracy $\varepsilon_{\mathrm{ACA}} > 0$ is satisfied.

The starting point of ACA is that every matrix of rank k is the sum of k matrices of rank 1. Thus, the idea at the basis of ACA algorithm is to improve the accuracy of the approximation by adding iteratively rank-1 matrices. At iteration k, the matrix $\mathbb{S}_k$ is constituted by k rows $\mathbf{q}_i$ and k columns $\mathbf{w}_i$, i.e.

$$\mathbb{S}_k := \sum_{i=1}^{k} \mathbf{q}_i \mathbf{w}_i^\top = \mathbb{Q} \cdot \mathbb{W}^\top. \tag{4.13}$$

The information is shifted iteratively from the residual to the approximant. More precisely, at iteration k, given $\mathbb{S}_k$ and assuming the row index $\tilde{m}^*$ is known the algorithm is given by the following six steps:

1. generation of the rows $\mathbf{a} := \mathbb{E}^{(\ell)\top}\mathbf{e}_{\tilde{m}^*}$ and $\mathbb{R}_k^\top \mathbf{e}_{\tilde{m}^*} := \mathbf{a} - \sum_{i=1}^{k} (\mathbf{q}_i)_{\tilde{m}^*} \mathbf{w}_i$;
2. find the column index $m^* := \mathrm{argmax}_m \left|(\mathbb{R}_k)_{\tilde{m}^*,m}\right|$ and compute $\gamma_{k+1} := (\mathbb{R}_k)^{-1}_{\tilde{m}^*,m^*}$;
3. generation of the columns $\mathbf{b} := \mathbb{E}^{(\ell)}\mathbf{e}_{m^*}$ and $\mathbb{R}_k\mathbf{e}_{m^*} := \mathbf{b} - \sum_{i=1}^{k} \mathbf{q}_i \, (\mathbf{w}_i)_{m^*}$;
4. find the next row index $\tilde{m}^* := \mathrm{argmax}_{\tilde{m}} \left|(\mathbb{R}_k)_{\tilde{m},m^*}\right|$;
5. compute vectors $\mathbf{q}_{k+1} := \gamma_{k+1}\mathbb{E}^{(\ell)}\mathbf{e}_{m^*}$ and $\mathbf{w}_{k+1} := \mathbb{E}^{(\ell)\top}\mathbf{e}_{\tilde{m}^*}$;
6. update the approximation $\mathbb{S}_{k+1} = \mathbb{S}_k + \mathbf{q}_{k+1}\mathbf{w}_{k+1}^\top$.

The algorithm stops when the new rank-1 approximation does not improve the accuracy of the approximation. Since at each iteration k, $\mathbb{S}_k - \mathbb{S}_{k-1} = \mathbf{q}_k\mathbf{w}_k^\top$ the stopping criteria reads

$$\|\mathbf{q}_k\|_2 \|\mathbf{w}_k\|_2 \leq \varepsilon_{\mathrm{ACA}} \|\mathbb{S}_k\|_{\mathrm{F}}. \tag{4.14}$$

As we can see, ACA provides a purely algebraic and easy to implement tool for the approximation of the energetic BEM blocks, without requiring any a priori kernel expansion.

Remark. Citing the work of Bebendorf (see [12, 13]), the ACA algorithm was original developed for asymptotic smooth kernels and for this class of operators its convergence and performances were theoretically investigated and assessed. Smooth kernels, like $\widetilde{V}(\mathbf{x}, \mathbf{y}; t)$, do not formally fit into the definition of asymptotic smoothness of a function. However, in this case the ACA algorithm can be interpreted as a rank-revealing decomposition applicable to kernels that admit degenerate approximations, as (4.3). At the authors' knowledge, one of the first application to smooth kernels can be found in [27].

Remark. Since the success of the proposed ACA based acceleration of the energetic BEM relies on the possibility of obtaining low-rank approximations of the blocks $\mathbb{E}^{(\ell)}$, we considered a set of such matrices related to a problem on a circumference Γ with unitary radius, approximated by $M = 512$ segments with length $\Delta x = \pi/256$, so that $\mathbb{E}^{(\ell)}$ is a 512-by-512 matrix. The problems evolves in the time interval $[0, 8\pi]$, decomposed uniformly with $N = 2048$ instants and characterized by the velocity $c = 1$. In the first row of Table 1, we report the evaluation of the ranks k_ℓ of some time blocks obtained by the execution of the ACA compression with threshold $\varepsilon_{\text{ACA}} = 1.0e-04$ in (4.14). These values are compared with the rank k_ℓ^* obtained by the estimate of the reminder, calculated for $r = 2$, i.e. the maximum value that this distance can assume on Γ, and by setting the threshold $\varepsilon = 1.0e-04$ in (4.11). The results confirm how the estimate of the rank by the study of the reminder of the decomposition (4.5) is qualitatively significant and they give us an idea of how low the rank of the blocks becomes as the time increases. We note that k_ℓ is bigger than k_ℓ^* but this phenomenon is not surprising since the ACA does not provide the best numerical rank but a good approximation. However, the two numerical ranks are of the same order.

ℓ	256	512	768	1024	1280	1536	1792	2048
k_ℓ	13	7	7	7	5	4	4	4
k_ℓ^*	11	4	3	2	2	2	2	1

Table 1: Comparison between the estimates of the ranks of $\mathbb{E}^{(\ell)}$ given by the execution of the ACA algorithm with threshold $\varepsilon_{\text{ACA}} = 1.0e-04$ in (4.14), and by the evaluation of the reminder $R_{k_\ell^*}(r; t_\ell)$ with threshold $\varepsilon = 1.0e-04$ in (4.11).

Formula (4.11) gives the possibility to know *a priori* an approximation of each block $\mathbb{E}^{(\ell)}$ low rank. Under slightly more restrictive hypothesis, we can give an upper bound for the low ranks of all the blocks to be compressed, not depending on the time index ℓ but only on the requested relative accuracy ε. Consequently, we will be able to give an upper bound of the overall computational cost of the marching-on-time procedure, based on the next result.

Proposition. Let $\lambda := \dfrac{\sqrt{3}\, diam(\Gamma)}{cT}$ be a real positive number depending on problem parameters and $\ell^* = \lceil \lambda N \rceil$ be the minimum natural number greater than or equal to λN. If $ct_{\ell^*} > \sqrt{3}\, diam(\Gamma)$, then for any fixed $\varepsilon > 0$, $\forall \ell \geq \ell^*$, the rank of block $\mathbb{E}^{(\ell)}$ can be bounded from above by the solution k_ε^* of the following inequality:

$$\frac{2(2k+3)!}{[(k+1)!]^2\, 12^{k+1}} < \varepsilon$$

and the computational cost of the ACA based compression scheme can be bounded from above by

$$2k_\varepsilon^*(1-\lambda)NM\,.$$

Proof. Looking at (4.7), we rewrite the related series at $t = t_\ell$, up to the sign, as $\sum_{k=0}^{+\infty} a_k$, with

$$a_k = \frac{\Delta x^2}{2\pi\,\ell^2}\,\frac{(2k+1)!}{(k!)^2 4^k}\,x^{2k}.$$

Since, due to the hypothesis, we have that $x \le \dfrac{diam(\Gamma)}{c\,t_{\ell^*}} < \dfrac{1}{\sqrt{3}}$, it holds for any $k \ge 0$

$$\frac{a_{k+1}}{a_k} = \left[1 + \frac{1}{2(k+1)}\right] x^2 \le \frac{3}{2}x^2 < \frac{1}{2} < 1$$

and we can bound from above the series reminder by

$$\frac{a_{k+1}}{1-\frac{1}{2}} = 2a_{k+1} \le \frac{\Delta x^2}{\pi\,\ell^2}\,\frac{(2k+3)!}{[(k+1)!]^2\,12^{k+1}}\,.$$

Finally, observing that (4.9) can be rewritten as

$$\frac{\Delta x^2}{2\pi\,\ell^2\,(1-x^2)^{\frac{3}{2}}}$$

we can impose a relative accuracy $\varepsilon > 0$ by

$$\frac{\frac{\Delta x^2}{\pi\,\ell^2}\,\frac{(2k+3)!}{[(k+1)!]^2\,12^{k+1}}}{\frac{\Delta x^2}{2\pi\,\ell^2\,(1-x^2)^{\frac{3}{2}}}} = 2\frac{(2k+3)!}{[(k+1)!]^2\,12^{k+1}}\,(1-x^2)^{\frac{3}{2}} < \frac{2(2k+3)!}{[(k+1)!]^2\,12^{k+1}} < \varepsilon\,.$$

The plot of the function $\dfrac{2(2k+3)!}{[(k+1)!]^2\,12^{k+1}}$ is given in Figure 2 and it is clear that we can solve the above chain last two members inequality, obtaining the searched upper bound $k = k_\varepsilon^*$ for the low rank of blocks $\mathbb{E}^{(\ell)}, \forall \ell \ge \ell^*$.

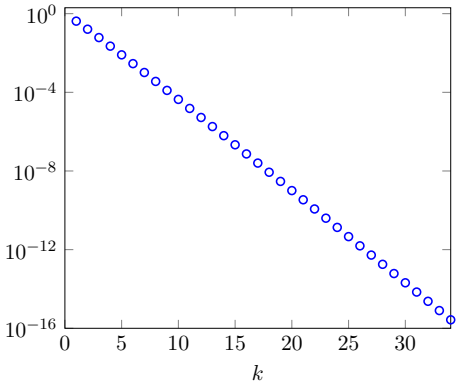

Figure 2: Plot of the function $\frac{2(2k+3)!}{[(k+1)!]^2\,12^{k+1}}$.

To conclude, the computational cost of the ACA based compression scheme can be bounded from above by

$$\sum_{\ell=\ell^*}^{N-1} 2k_\ell^* M \le 2\,k_\varepsilon^*(1-\lambda)\,NM\,.$$

□

Remark. For the N distinct time blocks in (3.5), the overall computational cost can be

bounded from above by

$$\sum_{\ell=0}^{\ell^*-1} f_\ell\, M + 2\, k_\varepsilon^*(1-\lambda)\, NM\,, \tag{4.15}$$

where f_ℓ, $\ell = 0, \cdots, \ell^* - 1$ are suitable coefficients such that $1 \leq f_\ell < M$. It is clear that, when $cT >> \sqrt{3}\, diam(\Gamma)$, the parameter λ and consequently ℓ^* tend to zero, and the above formula reduces to the second term. On the contrary, if $\lambda \to 1^-$, in principle one does not need blocks compression, because of the blocks sparsity pattern. Anyway, in this case and for blocks $\mathbb{E}^{(\ell)}$ related to growing values of coefficients f_ℓ, one can make use of well known compression algorithms for static problems (see e.g. [23, 24, 25]), due to (3.12) and its space singularity highlighted in (3.13) .

4.2. Elastodynamics

Observations similar to those made for the acoustic integration kernel can be made for the elastic problem and some of them are resumed below. We start by noting that, for growing time, the matrix element defined in (3.14) can be rewritten in the following reduced form

$$\left(\mathbb{E}_{ij}^{(\ell)}\right)_{\tilde{m},m} = -\frac{1}{2\pi\rho}\int_\Gamma w_{\tilde{m}}(\mathbf{x}) \int_\Gamma w_m(\mathbf{y})\widetilde{\mathcal{V}}_{ij}(\mathbf{x},\mathbf{y};t_\ell)\mathrm{d}\Gamma_{\mathbf{y}}\mathrm{d}\Gamma_{\mathbf{x}} \tag{4.16}$$

where the kernel

$$\begin{aligned}
\widetilde{\mathcal{V}}_{ij}(\mathbf{x},\mathbf{y};t) = \frac{\delta_{ij}}{2}\Bigg[&\frac{1}{c_{\mathrm{P}}^2}\log\left(\frac{\left(c_{\mathrm{P}}t+\sqrt{c_{\mathrm{P}}^2t^2-r^2}\right)^2}{\left(c_{\mathrm{P}}(t-\Delta t)+\sqrt{c_{\mathrm{P}}^2(t-\Delta t)^2-r^2}\right)\left(c_{\mathrm{P}}(t+\Delta t)+\sqrt{c_{\mathrm{P}}^2(t+\Delta t)^2-r^2}\right)}\right)\\
&+\frac{1}{c_{\mathrm{S}}^2}\log\left(\frac{\left(c_{\mathrm{S}}t+\sqrt{c_{\mathrm{S}}^2t^2-r^2}\right)^2}{\left(c_{\mathrm{S}}(t-\Delta t)+\sqrt{c_{\mathrm{S}}^2(t-\Delta t)^2-r^2}\right)\left(c_{\mathrm{S}}(t+\Delta t)+\sqrt{c_{\mathrm{S}}^2(t+\Delta t)^2-r^2}\right)}\right)\Bigg]\\
&+\frac{c_{\mathrm{P}}^2-c_{\mathrm{S}}^2}{c_{\mathrm{P}}c_{\mathrm{S}}}\left(\frac{r_ir_j}{r^2}-\frac{\delta_{ij}}{2}\right)\Bigg[\frac{2t}{c_{\mathrm{P}}\sqrt{c_{\mathrm{S}}^2t^2-r^2}+c_{\mathrm{S}}\sqrt{c_{\mathrm{P}}^2t^2-r^2}}\\
&-\frac{t+\Delta t}{c_{\mathrm{P}}\sqrt{c_{\mathrm{S}}^2(t+\Delta t)^2-r^2}+c_{\mathrm{S}}\sqrt{c_{\mathrm{P}}^2(t+\Delta t)^2-r^2}}-\frac{t-\Delta t}{c_{\mathrm{P}}\sqrt{c_{\mathrm{S}}^2(t-\Delta t)^2-r^2}+c_{\mathrm{S}}\sqrt{c_{\mathrm{P}}^2(t-\Delta t)^2-r^2}}\Bigg]
\end{aligned}$$

has the same properties of the reduced acoustic kernel $\widetilde{\mathcal{V}}(\mathbf{x},\mathbf{y};t)$, i.e. it is smooth for $r \to 0$ and symmetric w.r.t to the space variables. Moreover, for a fixed r, in the limit for $t \to \infty$ it tends to become identically zero. Since the generic matrix entry defined in (4.16) can be approximated as follows

$$\left(\mathbb{E}_{ij}^{(\ell)}\right)_{\tilde{m},m} \simeq -\frac{\Delta x^2}{2\pi\rho}\widetilde{\mathcal{V}}_{ij}(r;t_\ell), \tag{4.17}$$

we proceed with a generalised Taylor expansion in the vectorial variable $\mathbf{r} = (r_1, r_2)^\top$ of the right hand side of the previous relation, leading us to rewrite the element as a series of even terms:

$$\left(\mathbb{E}_{ij}^{(\ell)}\right)_{\tilde{m},m} \simeq \sum_{\substack{k=0\\|\boldsymbol{\alpha}|=2k}}^{\infty} \mathbf{C}_{\boldsymbol{\alpha}}^{ij}(t_\ell)\mathbf{r}^\alpha, \tag{4.18}$$

where the argument of the summation depends on a multi-index $\boldsymbol{\alpha} := (\alpha_1, \alpha_2)$ with $|\boldsymbol{\alpha}| = \alpha_1 + \alpha_2$, and $\mathbf{C}_{\boldsymbol{\alpha}}^{ij}(t)$ is a fourth-order tensor having a behaviour in time as $\mathcal{O}(1/(c_{\mathrm{S}}t)^{|\boldsymbol{\alpha}|+2})$. Consequently, we can conclude that the reduced elastodynamic kernels $\widetilde{\mathcal{V}}_{ij}(\mathbf{x},\mathbf{y};t)$ admit a low-rank expansion and that the ACA algorithm is applicable for the computation of the sub-blocks $\mathbb{E}_{ij}^{(\ell)}$, $i,j = 1,2$, in (3.7).

5. Numerical Results

This section consists of two main parts: the first is devoted to the numerical study of the efficiency of the proposed method, in terms of accuracy, memory saving and CPU time reduction; the second presents the application of the scheme to some soft scattering problems.

All the numerical computations have been performed on a cluster with two Intel® XEON® E5-2683v4 CPUs (2.1 GHz clock frequency and 16 cores) by means of parallel FORTRAN® codes.

5.1. Example 1. Numerical study of the efficiency of the proposed method.

Let Ω_0 be the unit disk centered at $(0,0)$, so that $\Gamma = \{\mathbf{x} \in \mathbf{R}^2 \ : \ \mathbf{x} = (\cos\theta, \sin\theta)^\top, \ \theta \in (-\pi, \pi]\}$. We consider the Problem (2.1) with the final time instant $T = 4\pi$.

Here, we aim at testing the accuracy and the efficiency of the approximations we obtain by using the energetic approach combined with the ACA technique. Since, to the best of our knowledge, for both the acoustic and the elastodynamic problems it is not possible to choose a Dirichlet datum $\mathbf{g}(\mathbf{x};t)$ such that an analytical expression of the exact solution of the problem is known, we construct the corresponding reference solution by solving the problem with the standard energetic BEM, by using M_e degrees of freedom for the space discretization and N_e sub-intervals for the time interval $[0, 4\pi]$. We refer to the reference solution as $\boldsymbol{\varphi}^*_{M_e,N_e}(\mathbf{x};t)$ and to the corresponding potential function as $\mathbf{u}^*_{M_e,N_e}(\mathbf{x};t)$, obtained replacing the analytical solution with $\boldsymbol{\varphi}^*_{M_e,N_e}(\mathbf{x};t)$ in the integral representation formula (2.3). Moreover, we denote by $\boldsymbol{\varphi}_{M,N}(\mathbf{x};t)$ and $\mathbf{u}_{M,N}(\mathbf{x};t)$ the approximate solution and the corresponding potential function obtained with the proposed ACA based acceleration, choosing the space and time discretization parameters M and N, respectively.

To test the accuracy of our method, we introduce the absolute error

$$E^{\boldsymbol{\varphi}}_{M,N} := \max_{t\in(0,T]} \left\| \boldsymbol{\varphi}^*_{M_e,N_e}(\cdot;t) - \boldsymbol{\varphi}_{M,N}(\cdot;t) \right\|_{L^2(\Gamma)}, \tag{5.1}$$

associated to the approximate solution $\boldsymbol{\varphi}_{M,N}(\mathbf{x};t)$, the error made on the calculation of the external solution at the point $\mathbf{x}_0 = (0,2)^\top$

$$E^{\mathbf{u}}_{M,N} := \max_{t\in(0,T]} \left| \mathbf{u}^*_{M_e,N_e}(\mathbf{x}_0;t) - \mathbf{u}_{M,N}(\mathbf{x}_0;t) \right|. \tag{5.2}$$

and the corresponding Estimated Order of Convergence (EOC), by means of the following standard formula:

$$\mathrm{EOC} := \log_2 \left| \frac{E^*_{M,N}}{E^*_{2M,2N}} \right| \qquad \text{with } * = \boldsymbol{\varphi}, \mathbf{u}. \tag{5.3}$$

Moreover, we focus our attention on the percentage of the memory saving, defined as

$$\mathrm{mem}(\%) := 100 \cdot \left(1 - \frac{1}{N} \sum_{\ell=0}^{N-1} \frac{k_\ell}{M} \right), \tag{5.4}$$

where k_ℓ/M is the ratio between the size of the compressed block $\mathbb{E}^{(\ell)}$ and the size of its complete (not compressed) form.

5.1.1. Acoustics

For the acoustic problem, we consider the Dirichlet boundary datum $g_1(\mathbf{x};t) = t^4 e^{-2t} \cos\left(x_1^2 + 2x_2^2\right)$ and $g_2(\mathbf{x};t) = 0$, so that $\varphi_2(\mathbf{x};t) = 0$. In the sequel, we report the numerical results corresponding to the parameters $M_e = 4096$ and $N_e = 8192$ for the computation of the reference solution. In spite of the previous underlined limitations of the standard energetic BEM, this choice of M_e and N_e is possible, because the considered geometry of Γ allows us to take advantage of the Toeplitz structure of the blocks $\mathbb{E}^{(\ell)}$, for $\ell = 0, 1, \ldots, N_e - 1$. Therefore, in this test we need to construct and store only the first row of each block. In Figure 3 and 4, we show the behaviour of the

component of $\boldsymbol{\varphi}^*_{M_e,N_e}(\mathbf{x};t)$ and $\mathbf{u}^*_{M_e,N_e}(\mathbf{x}_0;t)$ in the x_1-direction, for two values of the speed of wave propagation, i.e. $c=1$ and $c=343$.

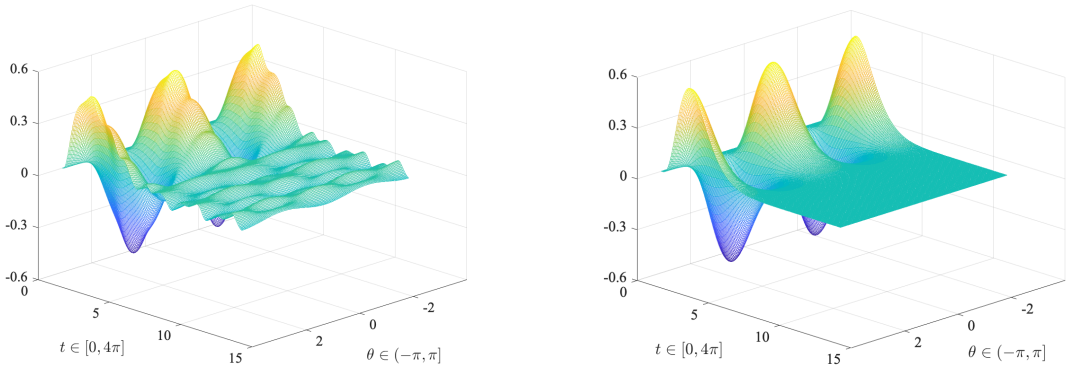

Figure 3: Acoustics. 3D view of the component in the x_1-direction of the reference density solution $\boldsymbol{\varphi}^*_{M_e,N_e}(\mathbf{x}(\theta);t)$ for $\theta \in (-\pi,\pi]$ and $t \in (0,4\pi]$, for two speeds of wave propagation, i.e. $c=1$ (left plot) and $c=343$ (right plot).

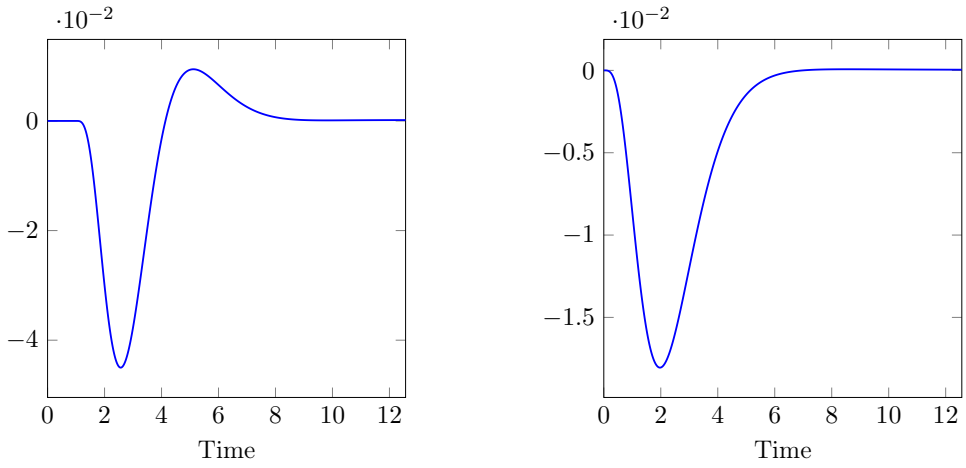

Figure 4: Acoustics. Time history of the component in the x_1-direction of the reference potential solution $\mathbf{u}^*_{M_e,N_e}((0,2)^\top;t)$ for $t \in (0,4\pi]$ and for two speeds of wave propagation, i.e. $c=1$ (left plot) and $c=343$ (right plot).

In Tables 2 and 3, we report the errors $E^{\boldsymbol{\varphi}}_{M,N}$ and $E^{\mathbf{u}}_{M,N}$, the corresponding EOCs and the percentages of memory saving, obtained by setting in (4.14) $\varepsilon_{\text{ACA}} = 1.0e-03$, $\varepsilon_{\text{ACA}} = 1.0e-04$ and $\varepsilon_{\text{ACA}} = 1.0e-05$ for the value of the speed of wave propagation $c=1$, and $\varepsilon_{\text{ACA}} = 1.0e-04$, $\varepsilon_{\text{ACA}} = 1.0e-05$ and $\varepsilon_{\text{ACA}} = 1.0e-06$ when we consider $c=343$.
We remark that we have obtained the same accuracy (at least up to the second significant digit) for all the considered choices of the threshold parameters, as well as for the standard (without ACA based compression) energetic BEM. This phenomenon is due to the fact that the highest value of the error is in the first time instants, whose corresponding blocks are stored in the standard (not compressed) format. On the other hand, as time passes, the blocks tends to become identically zero with decreasing rank and so their compression does not change the maximum error of the method, but they are necessary for the stability of the global procedure.
As we expected since we use constant shape functions in space and in time, we observe a linear convergence rate for the approximate density $\boldsymbol{\varphi}_{M,N}$. Indeed, the numerical results show a quadratic convergence rate for the approximate potential $\mathbf{u}_{M,N}$.
In Tables 2 and 3, the high memory saving obtained with the proposed compression technique is visible, too. We oberve that the memory saving improves when we increase the problem size. In particular, when we consider the speed of wave propagation $c=343$ and for the values $M=512$

and $N = 1024$, approximatively only 1.5% entries of the original matrices are needed for all the three considered parameters ε_{ACA}.

M	N	$E^{\boldsymbol{\varphi}}_{M,N}$	EOC	$E^{\mathbf{u}}_{M,N}$	EOC	mem $\varepsilon_{\text{ACA}} = 1.0e-03$	mem $\varepsilon_{\text{ACA}} = 1.0e-04$	mem $\varepsilon_{\text{ACA}} = 1.0e-05$
8	16	$2.67e-01$		$3.42e-02$		0.0%	0.0%	0.0%
			0.6		1.8			
16	32	$1.77e-01$		$9.87e-03$		12.5%	0.0%	0.0%
			1.0		1.9			
32	64	$8.47e-02$		$2.56e-03$		47.9%	39.0%	31.6%
			1.0		2.0			
64	128	$4.22e-02$		$6.28e-04$		66.1%	60.9%	57.6%
			1.0		1.7			
128	256	$2.03e-02$		$1.92e-04$		74.4%	72.1%	70.2%
			1.1		2.1			
256	512	$9.44e-03$		$4.41e-05$		78.4%	77.3%	76.4%
			1.2		2.0			
512	1024	$4.04e-03$		$1.09e-05$		80.3%	79.7%	79.4%

Table 2: Acoustics. Energetic BEM combined with the partially pivoted ACA. Absolute errors in L^2-norm of the boundary solution $\boldsymbol{\varphi}_{M,N}$ and absolute error of the external solution $\mathbf{u}_{M,N}$, with corresponding EOCs (speed of wave propagation $c = 1$).

M	N	$E^{\boldsymbol{\varphi}}_{M,N}$	EOC	$E^{\mathbf{u}}_{M,N}$	EOC	mem $\varepsilon_{\text{ACA}} = 1.0e-04$	mem $\varepsilon_{\text{ACA}} = 1.0e-05$	mem $\varepsilon_{\text{ACA}} = 1.0e-06$
8	16	$5.94e-01$		$8.54e-03$		37.5%	34.4%	25.0%
			0.7		0.4			
16	32	$3.54e-01$		$1.13e-02$		67.2%	65.6%	59.4%
			1.0		2.0			
32	64	$1.78e-01$		$2.83e-03$		84.6%	83.6%	83.6%
			1.0		2.0			
64	128	$8.95e-02$		$7.04e-04$		92.1%	91.5%	91.0%
			1.0		2.0			
128	256	$4.41e-02$		$1.78e-04$		96.0%	95.7%	95.0%
			1.0		2.0			
256	512	$2.13e-02$		$4.33e-05$		97.6%	97.5%	97.1%
			1.1		2.0			
512	1024	$9.93e-03$		$1.06e-05$		98.3%	98.2%	98.0%

Table 3: Acoustics. Energetic BEM combined with the partially pivoted ACA. Absolute errors in L^2-norm of the boundary solution $\boldsymbol{\varphi}_{M,N}$ and absolute error of the external solution $\mathbf{u}_{M,N}$, with corresponding EOCs (speed of wave propagation $c = 343$).

Note that for the choice of the parameters $N = 2M$ and speed of wave propagation $c = 1$ the Courant-Friedrichs-Lewy (CFL) number is $\beta = c\frac{\Delta t}{\Delta x} = 1.0$. However, applying for example the energetic BEM with $M = 512$ and $N = 4M$ ($\beta = 0.5$) or $N = M$ ($\beta = 2.0$), no instabilities appear, as shown in the plots of Figure 5. Thus, from this and many other numerical tests, the proposed method does not reveal instability problems, as proved in [3, 4], also in presence of ACA based compression. Percentages of memory saving for these simulations are given in Table 4: they are nearly the same, as expected from theoretical results given in Section 4, since in the simulations the variation is only related to the parameter N.

β	mem $\varepsilon_{\text{ACA}} = 1.0e-03$	mem $\varepsilon_{\text{ACA}} = 1.0e-04$	mem $\varepsilon_{\text{ACA}} = 1.0e-05$
0.5	80.4%	79.9%	79.4%
1.0	80.3%	79.7%	79.4%
2.0	80.5%	80.0%	79.5%

Table 4: Acoustics. Energetic BEM combined with the partially pivoted ACA. Percentages of memory saving for different CFL numbers (speed of wave propagation $c = 1$).

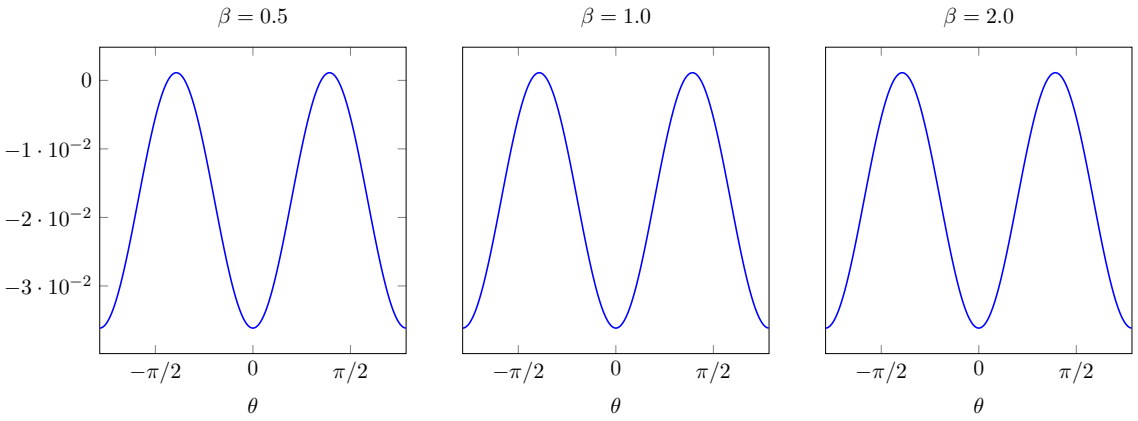

Figure 5: Acoustics. Component in the x_1-direction of the density solution $\boldsymbol{\varphi}_{M,N}(\mathbf{x}(\theta);T)$ for $\theta \in (-\pi,\pi]$, for the discretization parameters $M = 512$ and $N = 4M$ (left plot), $N = 2M$ (center plot) and $N = M$ (right plot).

The reduction of the memory requirement for the energetic BEM gives rise to an acceleration of the method even in terms of computation time. In the plots of Figure 6, we compare the CPU time needed by the standard energetic BEM and its ACA based acceleration for the computation of the blocks $\mathbb{E}^{(\ell)}$. The reported results are relative to the same discretization parameters and thresholds of Tables 2 and 3. For both the speeds of wave propagation $c = 1$ (left plot) and $c = 343$ (right plot), we underline that the growth of the CPU time (measured in seconds) is optimal, i.e. $\mathcal{O}(NM)$.

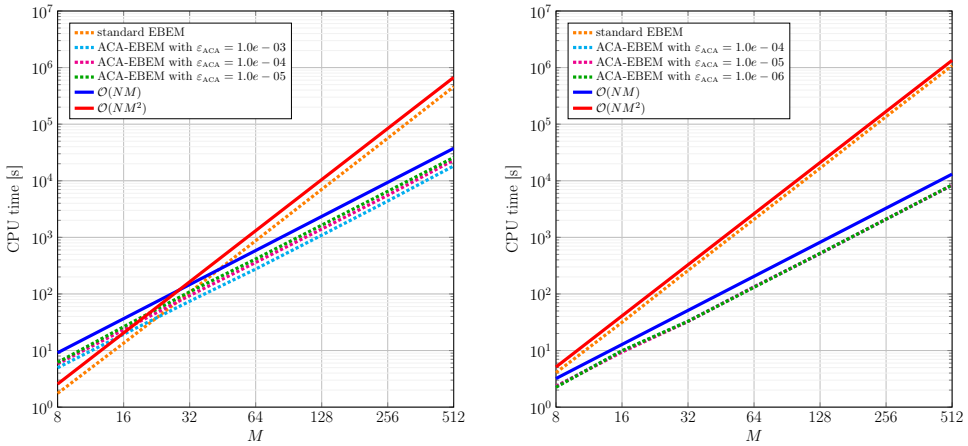

Figure 6: Acoustics. CPU time required to assemble the BEM system by the standard energetic BEM and its ACA based acceleration with different values of ε_{ACA}, for the speeds of wave propagation $c = 1$ (left plot) and $c = 343$ (right plot).For interpretation of the references to color in this figure, the reader is referred to the web version of this article.

Finally, in the plots of Figure 7 we show the behaviour in time of the absolute error

$$E^{\boldsymbol{\varphi}}(t) := \left\| \boldsymbol{\varphi}^*_{M_e,N_e}(\cdot;t) - \boldsymbol{\varphi}_{M,N}(\cdot;t) \right\|_{L^2(\Gamma)} \qquad t \in [0,4\pi],$$

where the reference and the approximate solutions are obtained by choosing the discretization parameters $M_e = M = 4096$ and $N_e = N = 8192$. In the left graph, the transient phase, where the blocks are stored in standard (not compressed) format, is cleary visible. For both the considered speeds of the wave propagation, we observe that, as time passes, the level of error introduced by the ACA can be controlled by the parameter ε_{ACA}, since the former is at most of the same order of magnitude of the latter.

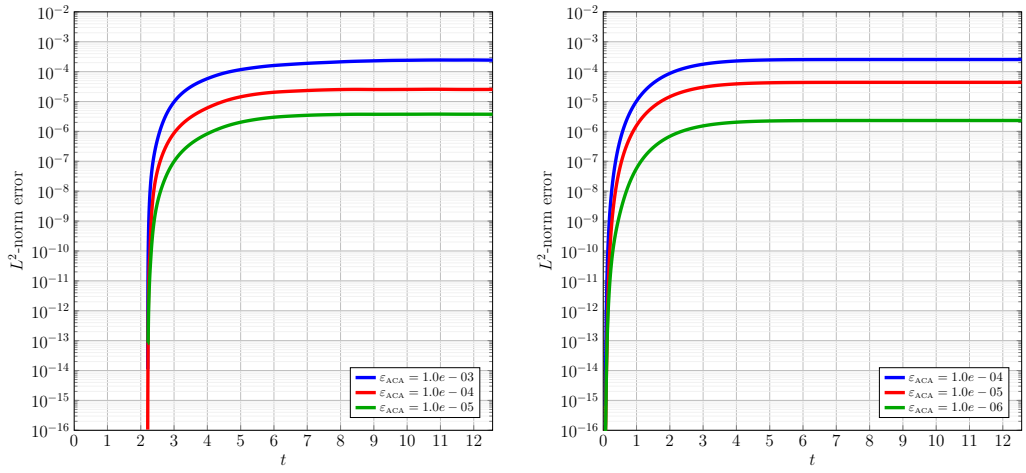

Figure 7: Acoustics. Time history of the error in L^2 norm on the solution of the BEM system. For interpretation of the references to color in this figure, the reader is referred to the web version of this article.

5.1.2. Elastodynamics

Now, we consider an exterior Dirichlet elastic problem with the velocities $c_{\mathrm{S}} = 1$ and $c_{\mathrm{P}} = 2$ and the datum $\mathbf{g}(\mathbf{x};t) = (g_1, g_2)^\top$, where

$$g_1(\mathbf{x};t) = t^4 e^{-2t} x_1 \quad \text{and} \quad g_2(\mathbf{x};t) = t^4 e^{-2t} x_2 \qquad \mathbf{x} \in \Gamma,\ t \in [0, 4\pi].$$

During our numerical testing, we have remarked that the blocks of the energetic BEM do not have the special Toeplitz structure underlined in the acoustic case. Therefore, we have to compute and store all their entries, so that we are limited in the choice of the reference parameters $M_e = 512$ and $N_e = 2048$. In Figure 8, we plot the two components of the reference solution $\boldsymbol{\varphi}^*_{M_e,N_e}(\mathbf{x};t)$ on Γ, while in Figure 9 we show only the vertical component of the reconstructed field $\mathbf{u}^*_{M_e,N_e}(\mathbf{x}_0;t)$ at the point $\mathbf{x}_0 = (0,2)^\top$, because the horizontal ones is null.

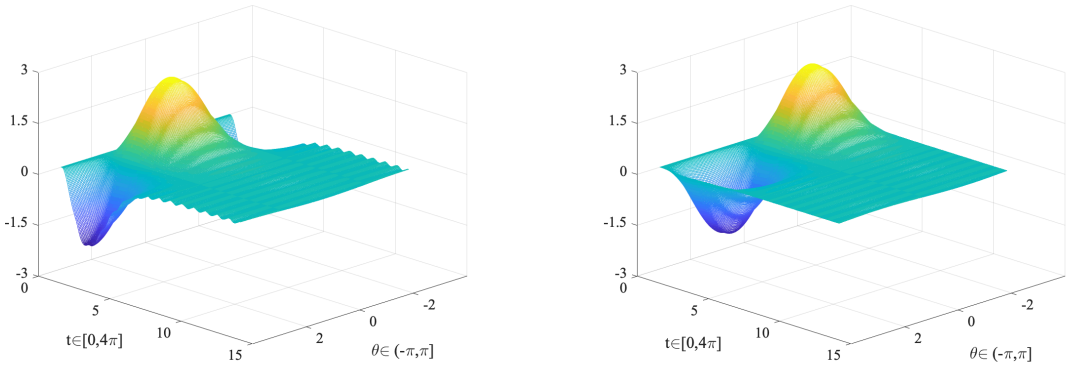

Figure 8: Elastodynamics. 3D view of the component in the x_1-direction (left plot) and in the x_2-direction (right plot) of the reference density solution $\boldsymbol{\varphi}^*_{M_e,N_e}(\mathbf{x}(\theta);t)$ for $\theta \in (-\pi,\pi]$, $t \in [0,4\pi]$ and the two speeds of wave propagation $c_{\mathrm{S}} = 1$ and $c_{\mathrm{P}} = 2$.

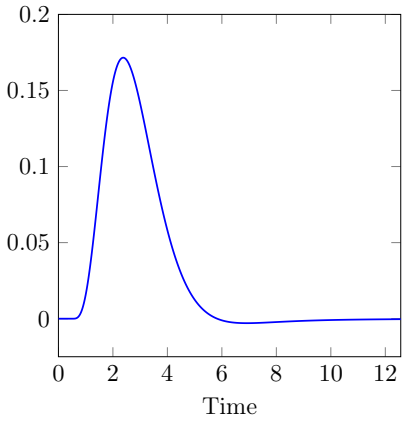

Figure 9: Elastodynamics. Time history of the component in the x_2-direction of the reference potential solution $\mathbf{u}^*_{M_e,N_e}((0,2)^\top;t)$ for $t \in (0,4\pi]$ and the two speeds of wave propagation $c_{\mathrm{S}} = 1$ and $c_{\mathrm{P}} = 2$.

In Table 5 we report the errors $E^{\boldsymbol{\varphi}}_{M,N}$ and $E^{\mathbf{u}}_{M,N}$, the corresponding estimated order of convergence (EOC) and the memory saving for three different values of the threshold parameter in (4.14), i.e. $\varepsilon_{\mathrm{ACA}} = 1.0e-03$, $\varepsilon_{\mathrm{ACA}} = 1.0e-04$ and $\varepsilon_{\mathrm{ACA}} = 1.0e-05$.

M	N	$E^{\boldsymbol{\varphi}}_{M,N}$	EOC	$E^{\mathbf{u}}_{M,N}$	EOC	mem $\varepsilon_{\mathrm{ACA}} = 1.0e-03$	mem $\varepsilon_{\mathrm{ACA}} = 1.0e-04$	mem $\varepsilon_{\mathrm{ACA}} = 1.0e-05$
8	32	$6.29e-01$		$1.81e-02$		0.0%	0.0%	0.0%
			1.0		1.9			
16	64	$3.11e-01$		$4.81e-03$		13.8%	0.0%	0.0%
			1.1		2.2			
32	128	$1.49e-01$		$1.07e-03$		48.4%	38.7%	30.5%
			1.2		1.9			
64	256	$6.44e-02$		$2.88e-04$		65.0%	60.2%	55.9%
			1.5		2.4			
128	512	$2.15e-02$		$5.35e-05$		73.2%	71.0%	68.3%

Table 5: Elastodynamics. Energetic BEM combined with the partially pivoted ACA. Absolute errors in L^2-norm of the boundary solution $\boldsymbol{\varphi}_{M,N}$ and absolute error of the external solution $\mathbf{u}_{M,N}$, with corresponding EOCs (speeds of wave propagation $c_{\mathrm{S}} = 1$ and $c_{\mathrm{P}} = 2$).

As in the acoustic case, the choice of the parameter $\varepsilon_{\mathrm{ACA}}$ does not influence the errors but only the memory saving. Furthermore, the EOCs reported in the above table confirm the first order convergence rate for the density function $\boldsymbol{\varphi}$ and the second order convergence rate for the solution $\mathbf{u}$. By comparing the results reported in Tables 2 and 5 we note the same level of accuracy and memory saving of the method for both the acoustic and the elastic models. As a consequence of the reduction of the memory requirement for the energetic BEM, we have an acceleration of the construction of the time blocks. In Figure 10 we show that the CPU time (measured in second) needed to assemble the energetic BEM system is proportional to NM, where the values of the discretization parameters are the same of the ones in Table 5.

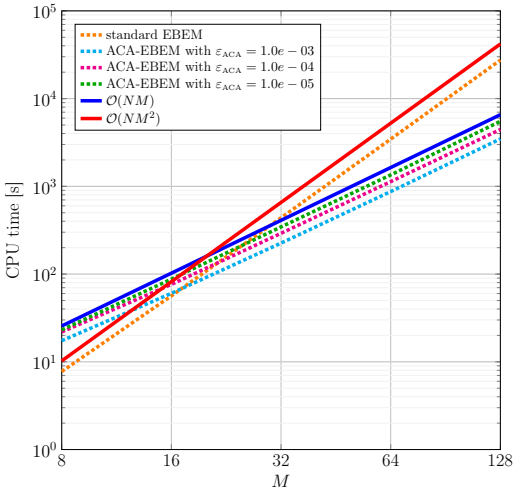

Figure 10: Elastodynamics. CPU time required to assemble the BEM system by the standard energetic BEM and its ACA based acceleration with different values of ε_{ACA}, for the speeds of wave propagation $c_{\text{S}} = 1$ and $c_{\text{P}} = 2$.For interpretation of the references to color in this figure, the reader is referred to the web version of this article.

Finally, in Figure 11 we show the time history of the absolute L^2-error between the approximate solution $\boldsymbol{\varphi}^*_{M_e,N_e}(\mathbf{x};t)$ obtained with the standard energetic BEM, and the approximate solution $\boldsymbol{\varphi}_{M,N}(\mathbf{x};t)$ obtained with the proposed ACA based acceleration, for the choice of the discretization parameters $M_e = M = 512$ and $N_e = N = 2048$. We have considered three different values of the threshold ε_{ACA} and, as in the acoustic case, the order of the error on the solution of the BEM system turns out to be the controlled by the fixed parameter.

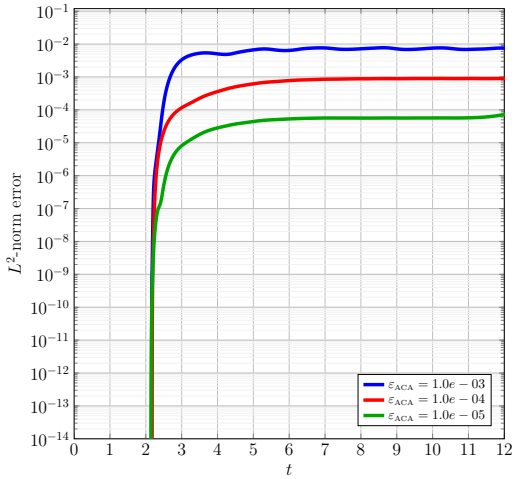

Figure 11: Elastodynamics. Time history of the error in L^2 norm on the solution of the BEM system. For interpretation of the references to color in this figure, the reader is referred to the web version of this article.

5.2. Example 2. Application to scattering problems.

A relevant field where the results in this work apply is in the study of the scattering of acoustic and elastic waves in homogeneous materials. Here, we consider the scattered field of a plane wave impinging upon an infinitely long cylindrical scatterer. In a fixed 3D Cartesian coordinates system $(x_1, x_2, x_3)^\top$, the cylindrical scatter is supposed to be invariant with respect to x_3. We suppose that the incident wave is simultaneously emitted by all the points in a line source parallel to the x_3-axis. Therefore, the incident wave is invariant to x_3 and the problem is reduced to a 2D case. Consequently, we choose to set our simulations in the plane $x_3 = 0$. The total wave field $\mathbf{u}_{\text{tot}}$ is given by the sum of the incident wave $\mathbf{u}_{\text{inc}}$ and the scattered one $\mathbf{u}_{\text{sca}}$, where the latter is the solution of problem (2.1) with the Dirichlet datum $\mathbf{g}(\mathbf{x};t) = -\mathbf{u}_{\text{inc}}(\mathbf{x};t)$ on the boundary Γ of the section of the scatterer.

5.2.1. Acoustics. Cylindrical scatterer with circular-shaped section.

In the first acoustic example we assume that Γ is a circumference of unitary radius centred in $(0,0)^\top$, scattered by a wave packet

$$\mathbf{u}_{\text{inc}}(\mathbf{x};t) = \left(\sum_{i=1}^{4} e^{-2(x_1-\xi_i+c(t+t_0))^2}, 0\right)^\top \qquad \text{with } t_0 = 0.13 \text{ and } \xi_i = 50, 55, 60, 65,$$

consisting of a sum of four successive waves spaced at regular intervals and travelling in x_1-direction with velocity $c = 343$. We solve the problem in the time interval $[0, 0.15]$ by means of the ACA based acceleration of the energetic BEM. For the space discretization we set the parameter $M = 128$, while the time interval of interest is subdivided into $N = 1049$ subintervals. In this numerical test the ACA threshold is $\varepsilon_{\text{ACA}} = 1.0e-04$ with a consequently memory saving of 87.3%.

In Figure 12, we show the snapshots of the total field at different instants and at the x_1x_2-domain $[-4,4] \times [-4,4]$ external to the obstacle.

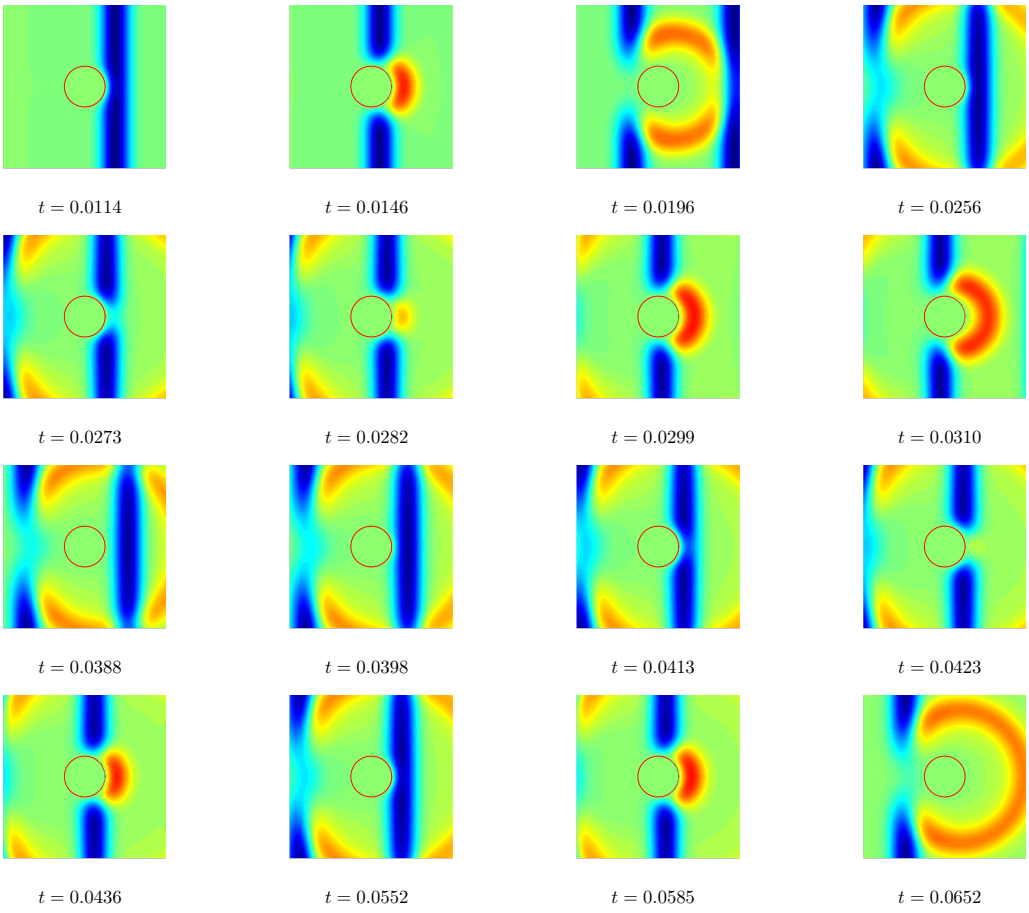

Figure 12: Acoustic scattering problem. Snapshots of the reconstructed total field $\mathbf{u}_{\text{tot}}$ around the circular-shaped section at different time instants.

5.2.2. Acoustics. Cylindrical scatterer with helicoidal-shaped section.

Now, we consider an acoustic wave generated by a single horizontally propagating incident wave:

$$\mathbf{u}_{\text{inc}}(\mathbf{x};t) = \left(e^{-50(x_1-50+c(t+0.13))^2}, 0\right)^\top$$

impinging on the obstacle, whose section Γ is given by the parametric representation:

$$\begin{cases} x_1 &= \rho(\theta)\cos\theta \qquad \theta \in (-\pi, \pi] \\ x_2 &= \rho(\theta)\sin\theta, \end{cases}$$

where

$$\rho(\theta) = 1 + \frac{1}{2}\cos(6\theta).$$

We refer to a medium where the wave propagation velocity is $c = 343$. We subdivide the time interval of interest $[0, 0.07]$ into $N = 10352$ instants while, for the space discretization, we choose to decompose the parametric interval $(-\pi, \pi]$ in $M = 4096$ sub-intervals. We set the threshold parameter $\varepsilon_{\text{ACA}} = 1.0e-04$. In spite of a bigger obstacle diameter and a halved final time instant of analysis with respect to the previous simulation, the compression efficiency, in this example involving a high number of degrees of freedom, is maintained at 86.2%. In the plots of Figure 13, we represent the behaviour of the reconstructed total field at different instants and at the x_1x_2-domain $[-4, 4] \times [-4, 4]$ external to the obstacle. As we can see, the proposed method allows the reproduction of an extremely complex scattered field given by the superposition of different waves.

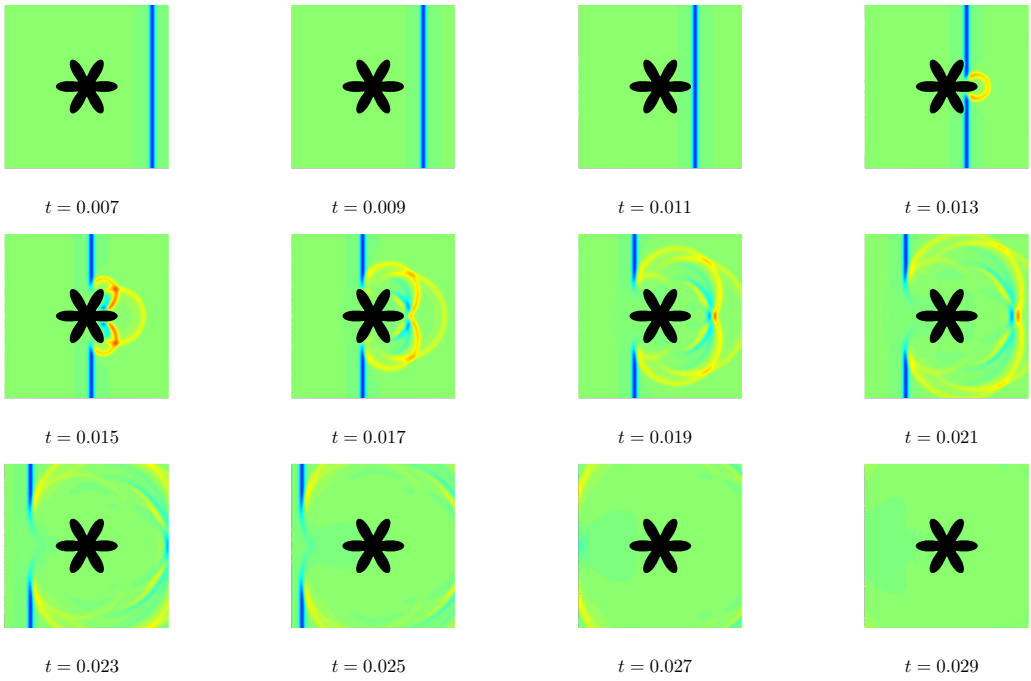

Figure 13: Acoustic scattering problem. Snapshots of the reconstructed total field $\mathbf{u}_{\text{tot}}$ around the helicoidal-shaped section of the obstacle at different time instants.

5.2.3. Elastodynamics

In the last example we aim at simulating an elastic wave generated by the incident P-wave

$$\mathbf{u}_{\text{inc}}(\mathbf{x}; t) = \left(e^{-20(x_1 - 2 + c_{\text{P}}t - 0.475)^2}, 0\right)^\top,$$

when the section of the obstacle is a circumference of unitary radius centred in $(0, 0)^\top$. Since in many elastic materials the Poisson's relation holds, i.e. $\lambda = \mu$, we assume $c_{\text{S}} = 1$ and $c_{\text{P}} = \sqrt{3}$. The spatial discretization parameter used to compute the approximate solution is $M = 128$ and we fix $N = 426$ equi-spaced time instants within the interval $[0, 12]$. The threshold parameter is $\varepsilon_{\text{ACA}} = 1.0e-04$ that gives rise to a memory saving of 71.1%.

In Figures 14 and 15 we present several snapshots related to the components in x_1- and x_2-directions, respectively, of the reconstructed total field in a square around the obstacle for different time instants. As expected, the vertical component appears once the solution in x_1-direction, generated by the given Dirichlet datum, bumps against the obstacle and is reflected back.

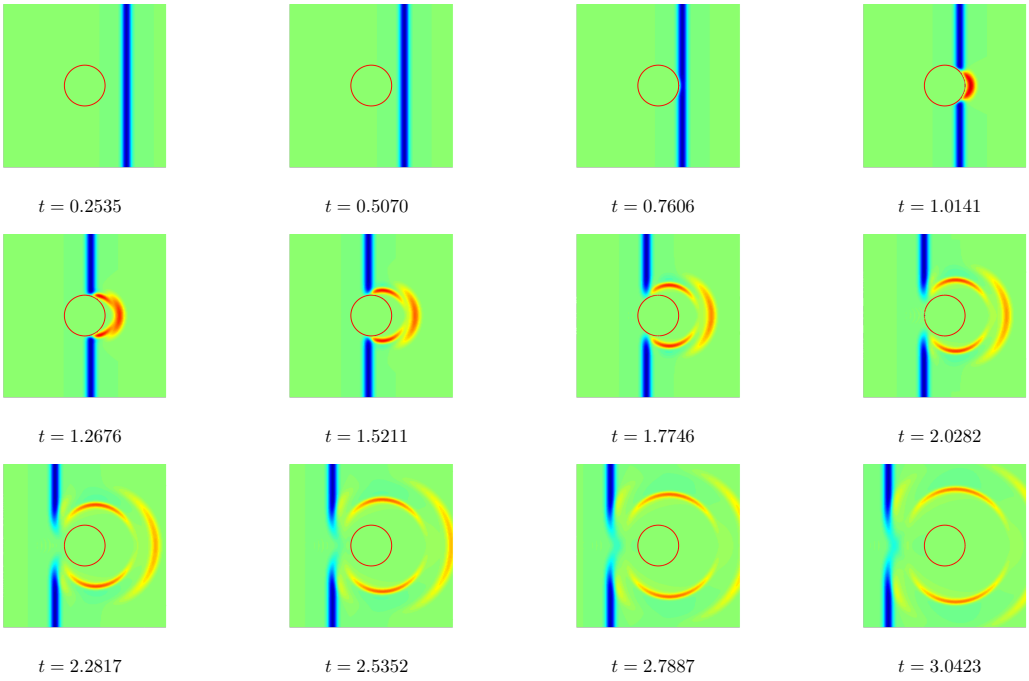

Figure 14: Elastodynamic scattering problem. Circular-shaped section. Snapshots of the component in the x_1-direction of the reconstructed total field $\mathbf{u}_{\text{tot}}$ around the obstacle at different time instants.

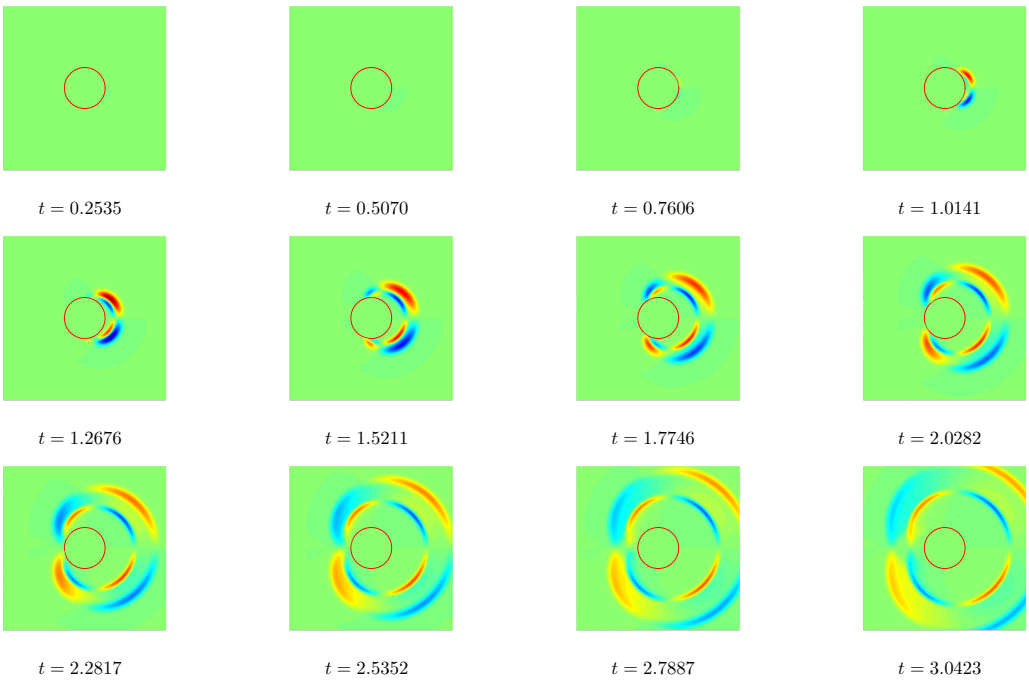

Figure 15: Elastodynamic scattering problem. Circular-shaped section. Snapshots of the component in the x_2-direction of the reconstructed total field $\mathbf{u}_{\text{tot}}$ around the obstacle at different time instants.

Finally, we change the geometry of the section of the obstacle and we assume that Γ is a kite described by the parametric equations:

$$\begin{cases} x_1 & = \cos\theta + 0.65\cos 2\theta - 0.65 \qquad \theta \in (-\pi, \pi] \\ x_2 & = 1.5\sin\theta, \end{cases}$$

In Figures 16 and 17 we show the component of the total field in the x_1 and x_2 directions, respectively, at the same time instants of the previous simulation. In this case the approximate density solution has been obtained by a decomposition of the parametric interval into $M = 2048$ sub-intervals, while the time discretization has been performed by using $N = 7095$ time steps. The chosen threshold parameter for the compression of the time blocks is $\varepsilon_{ACA} = 1.0e-04$. In spite of a bigger obstacle diameter with respect to the previous geometry, we observe also in this example, involving a high number of degrees of freedom, a memory saving of 72.5%. This saving percentage increases to 76.0% when we deal with a simulation with $M = 8192$ and $N = 28380$, confirming the efficiency of the proposed approach.

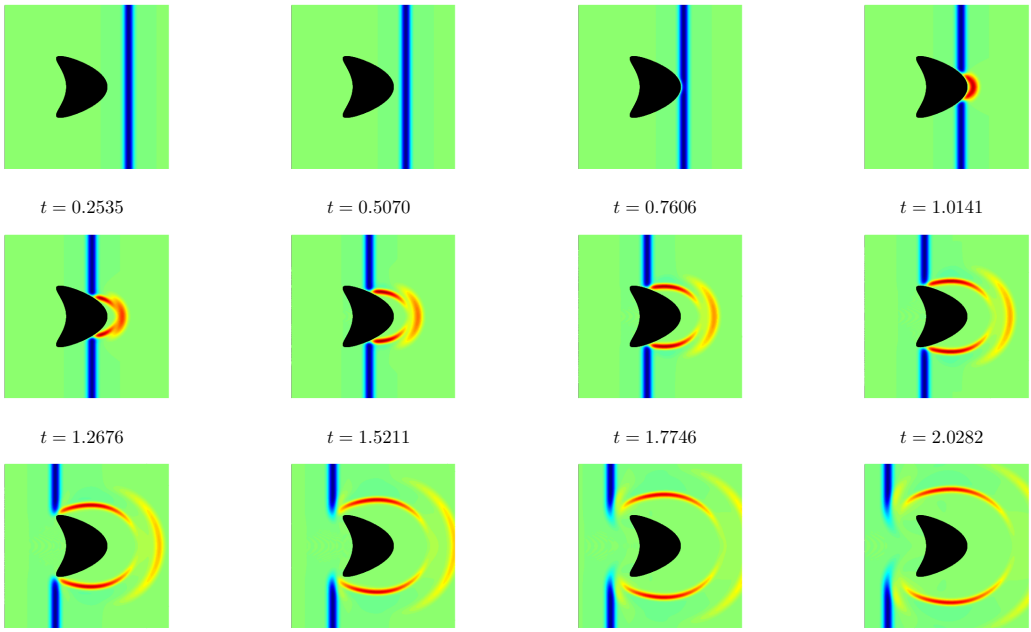

Figure 16: Elastodynamic scattering problem. Kite-shaped section. Snapshots of the component in the x_1-direction of the reconstructed total field $\mathbf{u}_{\text{tot}}$ around the obstacle at different time instants.

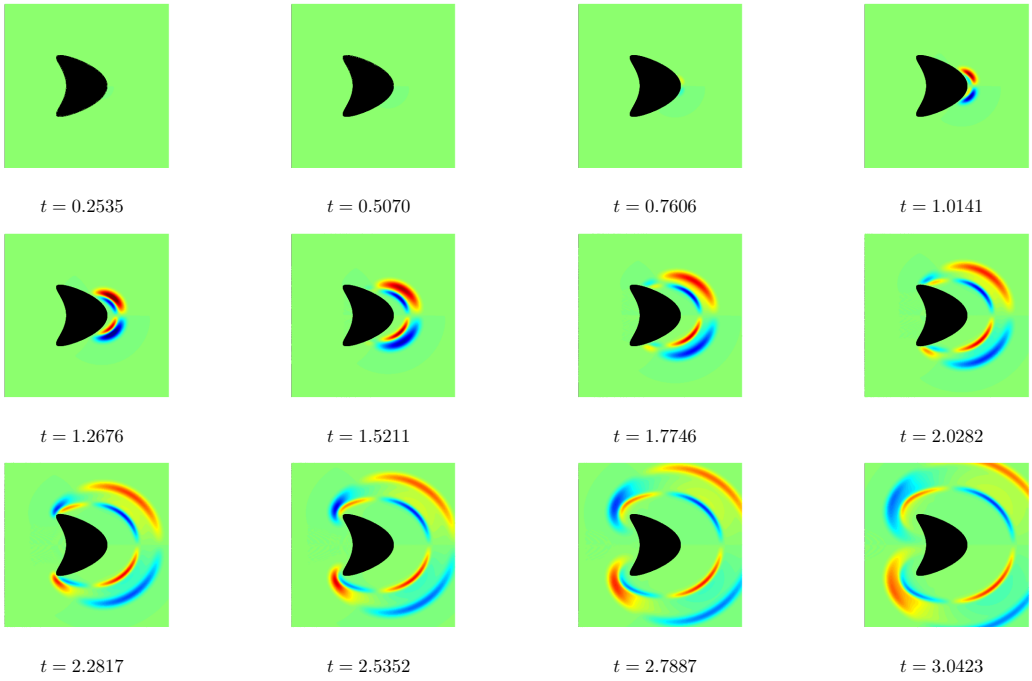

Figure 17: Elastodynamic scattering problem. Kite-shaped section. Snapshots of the component in the x_2-direction of the reconstructed total field $\mathbf{u}_{\text{tot}}$ around the obstacle at different time instants.

6. Conclusions and prespectives

We have considered a boundary integral reformulation of the 2D time-domain acoustic and elastic wave problems, to which one can eventually reduce 3D problems invariant in one of the cartesian directions. In particular, we have focused our attention on problems defined in unbounded regions, external to bounded obstacles, and endowed by a Dirichlet type boundary condition. For the resolution of the corresponding Boundary Integral Equation, we have used the space-time energetic Galerkin Boundary Element Method. The novelty of this paper consists in applying the partially pivoted version of the Adaptive Cross Approximation technique to reduce the computational time and the memory requirement for the matrix blocks of the resulting global discretization. The proposed numerical procedure allows for a compression of the energetic BEM blocks without the need of storing a priori the fully populated ones. Out of an extensive numerical testing, the results we have obtained show the optimality of the global scheme and reveal it to be accurate and competitive in terms of memory saving and CPU time.
We believe that the proposed approach displays potentials also for what concerns the application of the energetic BEM method to 3D realistic and seismic oriented cases, where the compression of the blocks is even more crucial. An investigation in this direction is underway.
Finally, we remark that at the current stage the design and the implementation of a fast, stable and accurate solver, that allows to increase the capabilities of the energetic BEM, are still open questions. Even if this issue is crucial to successful applications of the proposed method to large-scale HPC applications, it is out of the aim of the present pioneering paper. Since these aspects are worth to be studied, they will be the subject of future investigations.

Acknowledgments

The authors are grateful to the referees for their careful reading of the manuscript and their useful comments. This research benefits from the HPC (High Performance Computing) facility of the University of Parma, Italy.

Funding

This work was performed as part of the GNCS-INdAM 2020 research program *"Metodologie innovative per problemi di propagazione di onde in domini illimitati: aspetti teorici e computazionali"*. The University of Parma is supporting first and the third authors under project Fil2020 - Action A1 *"Time-domain Energetic BEM for elastodynamic problems, with advanced application"*, and the second author under the project Fil2020 - Action B *"A fast space-time BEM approach for scattering vector problems in 3D"*.

References

[1] T. Abboud, J.C. Nédélec, J. Volakis *Stable solution of the retarded potential equations*, in: Proceedings of the 17th ACES Conference, Monterey, CA, (2001), 146–151.

[2] A. Aimi, M. Diligenti, C. Guardasoni, I. Mazzieri, S. Panizzi, *An energy approach to space-time Galerkin BEM for wave propagation problems*, International Journal for Numerical Methods in Engineering, **80**(9), (2009), 1196–1240.

[3] A. Aimi, S. Panizzi, *BEM-FEM coupling for the 1D Klein-Gordon equation*, Numerical Methods for Partial Differential Equations, **30**, (2014), 2042–2082.

[4] A. Aimi, M. Diligenti, A. Frangi, C. Guardasoni, *Energetic BEM-FEM coupling for wave propagation in 3D multidomains*, International Journal for Numerical Method in Engigneering, **97**, (2014), 377–394.

[5] A. Aimi, L. Desiderio, M. Diligenti, C. Guardasoni, *Application of energetic BEM to 2D elastodynamic soft scattering problems*, Communications in Applied and Industrial Mathematics, **10**(1), (2019), 182–198.

[6] A. Aimi, L. Desiderio, P. Fedeli, A. Frangi, *A fast boundary-finite element approach for estimating anchor losses in micro-electro-mechanical system resonators*, Applied Mathematical Modelling, **97**, (2021), 741–753.

[7] A. Aimi, G. Di Credico, H. Gimperlein, E.P. Stephan, *Higher-order time domain boundary elements for elastodynamics - graded meshes and hp-versions*, Numerische Mathematik, (2021), under review.

[8] A. Aimi, G. Di Credico, M. Diligenti, C. Guardasoni, *Highly accurate quadrature schemes for singular integrals in energetic BEM applied to elastodynamics*, Journal of Computational and Applied Mathematics, **410**, (2022), 114186.

[9] B. Alpert, G. Beylkin, R. Coifman, V. Rokhlin, *Wavelet-like bases for the fast solutions of second-kind integral equations*, SIAM Journal on Scientific Computing, **14**(1), (1993), 159–184.

[10] L. Andersen, *Linear Elastodynamic Analysis*, Aalborg University, (2006).

[11] A. Bamberger, T. Ha Doung, *Formulation variationelle espace-temps pour le calcul par potentiel retardé da la difraction d'une onde acoustique*, Mathematical Methods in the Applied Sciences, **8**, (1986), 405–435.

[12] M. Bebendorf, *Approximation of boundary element matrices*, Numerische Mathematik, **86**(4), (2000), 565–589.

[13] M. Bebendorf, S. Rjasanow, *Adaptive low-rank approximation of collocation matrices*, Computing, **70**, (2003), 1–24.

[14] S. Bertoluzza, S. Falletta, L. Scuderi, *Wavelets and convolution quadrature for the efficient solution of a 2D space-time BIE for the wave equation*, Applied Mathematics and Computation, **366**, (2020), 124726.

[15] S. Chaillat, L. Desiderio, P. Ciarlet Jr, *Theory and implementation of $\mathcal{H}$-matrix based iterative and direct solvers for oscillatory kernels*, Journal of Computational Physic, **351**, (2017), 165–186.

[16] M. Costabel, *Time-dependent problems with the boundary integral equation method*, Encyclopedia of computational mechanics, **1**, (2004), 703–721.

[17] L. Desiderio, *An $\mathcal{H}$-matrix based direct solver for the Boundary Element Method in 3D elastodynamics*, AIP Conference Proceedings, **1978**, (2018), 120005.

[18] L. Desiderio, S. Falletta *Efficient Solution of Two-Dimensional Wave Propagation Problems by CQ-Wavelet BEM: Algorithm and Applications*, SIAM Journal on Scientific Computing, **42**(4), (2020), B894-B920.

[19] A.C. Eringer, E.S. Suhubi, *Elastodynamics*, Academic Press, New York, (1975).

[20] S. Falletta, S. Sauter, *The panel-clustering method for the wave equation in two spatial dimensions*, Journal of Computational Physics, **305**, (2016), 217–243.

[21] D. Givoli, High-order local non-reflecting boundary conditions: a review, *Wave Motion*, **39** (2004), pp. 319–326.

[22] D. Givoli, Numerical Methods for Problems in Infinite Domains. *Elsevier*, (2013).

[23] L. Greengard, V. Rokhlin, *A fast algorithm for particle simulations*, Journal of Computational Physics, **73**(2), (1987), 325–348.

[24] W. Hackbusch, Z.P. Nowak *On the fast matrix multiplication in the boundary element method by panel clustering*, Numerische Mathematik, **54**(4), (1989), 463–491.

[25] W. Hackbusch, A sparse arithmetic based on $\mathcal{H}$-Matrices. Part I: Introduction to $\mathcal{H}$-Matrices, Computing, **62**, (1999), 89–108.

[26] C. Lubich, *On the multistep time discretization of linear initial-boundary value problems and their boundary integral equations*, Numerische Matematik, **67**, (1994), 365–389.

[27] T. Mach, L. Reichel, M. Van Barel, R. Vandebril, *Adaptive cross approximation for ill-posed problems*, Journal of Computational and Applied Mathematics, **303**, (2016), 206–217.

[28] A. Quarteroni, A. Valli, *A Numerical Approximation of Partial Differential Equations*, Springer Verlag: Berlin, (1994).

[29] B. Shanker, A.A Ergin, K. Aygün, E. Michielssen *Analysis of transient electromagnetic scattering phenomena using a two-level plane wave time-domain algorithm*, IEEE Transactions on Antennas and Propagation, **48**(4), (2000), 510–523.

[30] M. Schanz, *Fast multipole method for poroelastodynamics*, Engineering analysis with boundary elements, **89**, (2018), 50–59.

[31] V.S. Vladimirov, *Equations of Mathematical Physics*, MIR, Moscow Russia, (1984).